INVESTIGATING THE USE OF GEOPHYSICAL TECHNIQUES TO DETECT HYDROCARBON SEEPS

By

VINCENT TAMBWE SOMWE

Bachelor of Mineral Science

University of Zambia

Lusaka, Zambia

1998

Submitted to the Faculty of the
Graduate College of the
Oklahoma State University
in partial fulfillment of
the requirements for
the Degree of
MASTER OF SCIENCE
December, 2015

INVESTIGATING THE USE OF GEOPHYSICAL

TECHNIQUES TO DETECT HYDROCARBON SEEPS

Thesis Approved:

Dr. Estella A. Atekwana

Thesis Adviser

Dr. Mohamed G. Abdelsalam

Dr. Jeffrey M. Byrnes

.

ACKNOWLEDGEMENTS

*"**Blessing, and honour, and glory, and power, be unto him that sitteth upon the throne**" Rev:4-6 (KJV).*

Thank you to Drs Estella and Eliot Atekwana, Dr Abdel Salam Mohamed, Dr Jeffrey Byrnes, Dr Jim Puckette for their guidance and advices.

Thank you to all OSU colleagues and especially to Andrew Katumwehe, Luel Emishaw, Kitso Matende, Achang Mercy, Meng Jingyao, Emmanuel Njinju and Tadesse Alemu for the team work.

*Utmost regards to **Ngalula B.Marie**, **Somwe M. Valentin** and Somwe Family for their support & Prayers. Regards to Sabah and El Kamchi Family for their Sacrifice.*

Thank you to Boone Pickens School of Geology for financial Support and thousands thanks to Alberta Student Aid and Government of Canada.

Name: Vincent T. Somwe

Date of Degree: December, 2015

Title of Study: INVESTIGATING THE USE OF GEOPHYSICAL TECHNIQUES TO DETECT HYDROCARBON SEEPS

Major Field: Geology

Abstract: In the Cement oil field, seeps occur in the Hydrocarbon Induced Diagenetic Aureole (HIDA). This 14 square km diagenetic alteration region is mainly characterized by the: (1) secondary carbonate minerals deposition that tends to form ridges throughout the oil field; (2) disseminated pyrite in the vicinity of the fault zones; (3) uranium occurrence and the change in color pattern from red to bleached red sandstone. Generally the HIDA of the Cement oil field is subdivided into four zones: (1) carbonate cemented sandstone zone (zone 1), (2) altered sandstone zone (zone 2), (3) sulfide zone (zone 3) and (4) unaltered sandstone zone (zone 4).

This study investigated the use of geophysical techniques to detect alteration zones over the Cement oil field. Magnetic and electromagnetic data were acquired at 5 m interval using the geometric G858 magnetometer and the Geonics EM-31 respectively. Both total magnetic intensity and bulk conductivity were found to decrease across boundaries between unaltered and altered sandstones. Boundaries between sulfide and carbonate zones, which in most cases were located in fault zones, were found to be characterized by higher magnetic and bulk conductivity readings. The contrast between the background and the highest positive peak was found to be in the range of 0.5-10% for total magnetic intensity and 258-450% for bulk conductivity respectively; suggesting that the detection of hydrocarbon seeps would be more effective with EM techniques.

The study suggests that geophysical techniques can be used to delineate contact between the different alteration zones especially where metallic minerals such as pyrite are precipitated. The occurrence of carbonate cemented sandstone in the Cement oil field can be used as a pathfinder for hydrocarbon reservoir. The change in color in the altered sandstone zone can still be useful in the hydrocarbon exploration.

TABLE OF CONTENTS

LIST OF TABLES

Table Page

LIST OF FIGURES

Figure Page

Figure Page

.

CHAPTER I

INTRODUCTION

1. Project motivation

The increasing demand for fossil fuels and the depletion of conventional reserves have motivated the search for new resources in frontier basins. One indicator of hidden hydrocarbon reservoir is the occurrence of hydrocarbon seeps at the surface. Throughout the world and throughout history, hydrocarbon seeps have proven to be reliable indicators of the presence of subsurface hydrocarbon reservoirs. The detection of physical, chemical and biological anomalies associated with hydrocarbon seepages is the basis of a number of exploration techniques that have accounted for several large discoveries (e.g., Cantarell fields, in the Gulf of Mexico) (Hubert et al., 2010). Different studies on Hydrocarbon Induced Diagenetic Aureoles (HIDA) agree that about 75% of the world's oil basins show hydrocarbon seepage (Clarke and Cleverly, 1991; Clayton et al., 1991; Williams and Lawrence, 2002; Barriol et al., 2006) and only 11 % of drilling on prospects without seepage results in new discoveries (Schumacher et al., 2011). This justifies in part why in most exploration programs, the detection of hydrocarbon seeps has become increasingly important especially in frontier basins (Sundberg, 1994).

2. Location of HIDAs in the US

Long term hydrocarbon seeps can induce diagenetic alterations that are mainly characterized by mineralogical changes (HIDA). There are many HIDAs that occur throughout the world. In the USA most of HIDA locations (Figure 1) are characterized by the change in the color pattern of the local soil. The precipitation of secondary carbonate minerals is one of the factors that justifies the change in color pattern in the vicinity of the seepage areas. In general, many alterations that take place in the seepage area are enhanced by microbial oxidation, under aerobic or anaerobic conditions (Yaron et al., 2012).

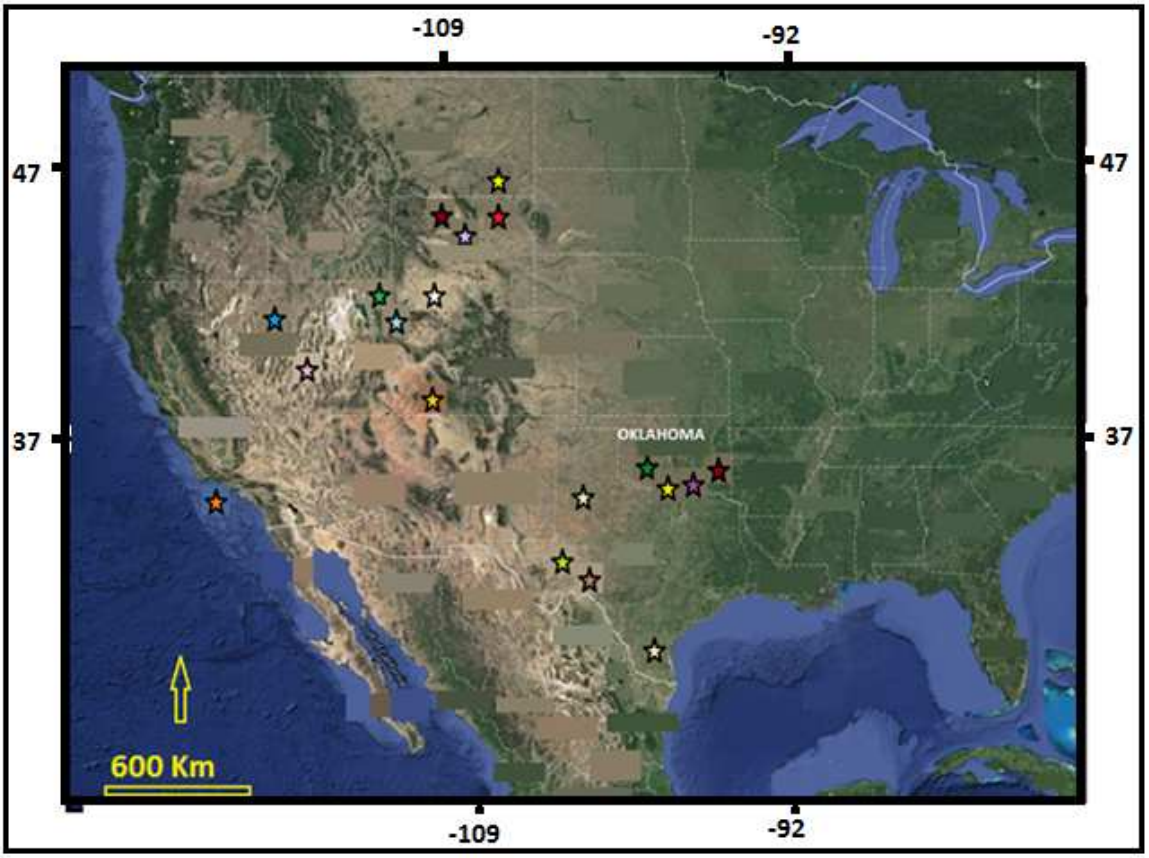

Figure 1: Location of Hydrocarbon Induced Diagenetic Alteration zones in USA. Each of the 21 oil fields is described by Yaron et al., (2012). US Map was adapted from www.google.com.The Cement oil field in the southwest of Oklahoma is represented by a green star.

3. Formation of hydrocarbon seeps and HIDA

Though the process of formation of hydrocarbon seeps is not fully understood, it is reasonable to believe that it is enhanced by the fracturing of cap rocks (Gluyas et al., 2004). Indeed there are several geological processes that can break down the cap rocks: (1) a rapid and anisotropic loading of fine grained sediments; (2) a dilation and reclose of micro fractures; (3) a local change in biophysical properties and consequently in the mineralogy (authigenic precipitation of pore-filling carbonate cements or even a conversion of weakly magnetic parent mineral into magnetite) (Stone et al., 2004).

4. Techniques for mapping HIDA

The potential to detect hydrocarbon seeps on the earth surface is based on the fact that areas of hydrocarbon seepages are characterized by " (1) microbiological anomalies and the formation of 'paraffin dirt'; (2) mineralogical changes such as formation of calcite, pyrite, uranium, elemental sulfur, and certain magnetic iron oxides and sulfides; (3) bleaching of red beds (4) clay mineral alteration; (5) electrochemical changes; (6) radiation anomalies; (7) biogeochemical and geobotanical anomalies" (Schumacher, 1996).

Bleaching of some stratigraphic horizons is the most visible feature that can be used for the detection of long term hydrocarbon seeps in the field, as well as on the satellite image. Usually the bleaching is due either to the secondary deposition of carbonate minerals or to the reduction of Fe^{3+} to Fe^{2+}.

4. 1 Remote sensing

In the Tian Shan basin in China, anomalous bleached regions related to hydrocarbon induced alteration were detected by an Advanced Spaceborne Thermal Emission and Reflection

Radiometer (ASTER) multispectral images. These results were in good agreement with mineral identification using X-ray diffraction (Fu et al., 2007).

The use of hyperion hyperspectral imaging sensors to map alterations that appear to be associated with hydrocarbon microseepages in the Patrick Draw area of Wyoming resulted in the successful identification of the hydrocarbon seepage areas. The imaging sensors results were supported by mineralogical and geochemical data (Khan et al., 2008).

The detection of hydrocarbon seeps by ASTER and hyperion hyperspectral imaging sensors have some limitations. This technique can only provide good results in areas with sparse vegetation cover (Fu et al., 2007) consequently, there is need to search for alternative techniques that can complement the ASTER multispectral image.

4. 2 Microbial techniques

In the search for more efficient techniques, microbial techniques (Figure 2) are increasingly used in the hydrocarbon exploration. These techniques are generally based on the detection of anomalous concentration of specific oxidizing bacteria that are associated with the presence of hydrocarbon. Basically the presence of hydrocarbon-oxidizing bacteria (HCO) plays an important role in soil samples as it is considered as an indication of hydrocarbon presence (Rasheed et al., 2013). The group of oxidizing bacteria that are usually associated with the presence of hydrocarbon comprise the genera of *Brevibacterium*, *Corynebacterium, Flavobacterium, Mycobacterium, Nocardia, Pseudomonas, Rhodococcus,* etc. (Perry and Williams, 1968; Vestal et al., 1971 and Rasheed et al., 2013). It is important to bear in mind that in addition to the species of oxidizing bacteria mentioned above, many types of microorganism possess the enzymatic capability to degrade petroleum products: Some types degrade alkanes and other degrade aromatics compounds (Perry and Williams, 1968).

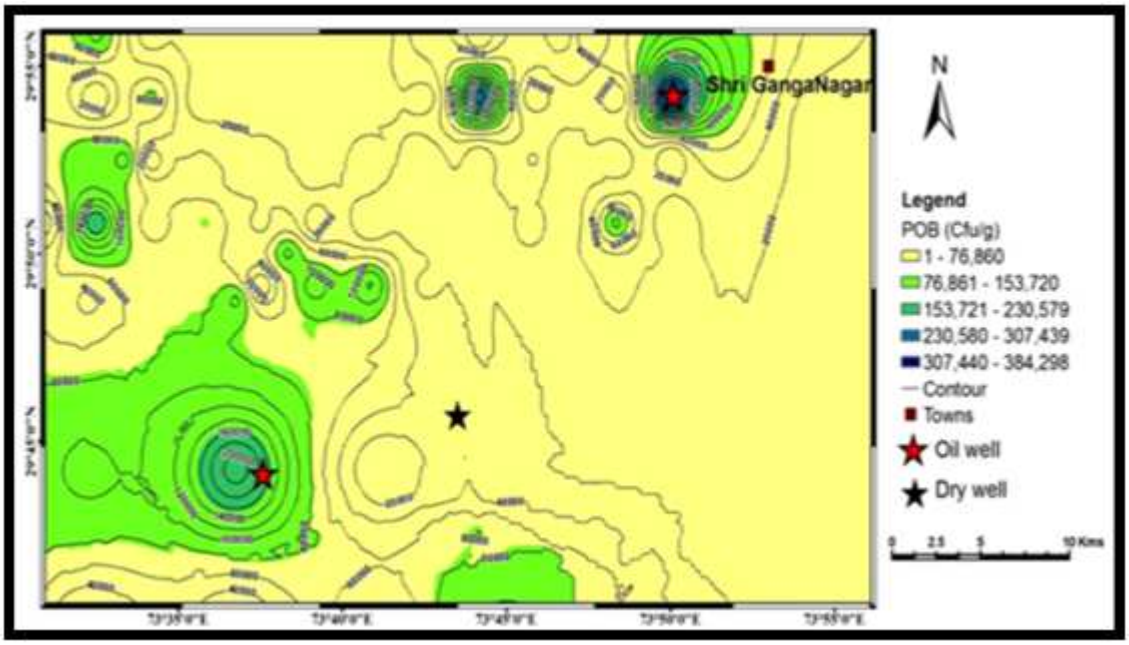

Figure 2: Anomaly of hydrocarbon oxidizing bacteria in Shri Ganga Nagar Block (Rajasthan Basin), in India. Modified from Rasheed et al. (2013).

Though the success rate of microbial prospecting survey has been reported to be 90% (Rasheed et al., 2013), microbial techniques are always integrated with geological, geochemical and geophysical methods. Indeed microbial techniques can be laborious and extremely expensive, especially if they have to include non-prospecting areas (Desai et al., 2006).

4. 3 Geochemical Techniques

There are many similarities between the geochemical techniques and the microbial techniques. Instead of targeting anomalous concentration of oxidizing bacteria, geochemical techniques are concerned with the detection of anomalous concentration of light hydrocarbon (methane up to butane) that diffuses through a porous horizon overlying hidden hydrocarbon reservoir. Light hydrocarbon can also seep through a network of fractures (Figure 3). The presence of ring Pac such as naphthalene plays an important role in the identification of the type of hydrocarbon reservoir (Cannon et al., 2001).

In short, the fact that light hydrocarbons such as methane, ethane up to butane can ascend quickly up to the surface through networks of discontinuities even when these discontinuities are filled

with water, makes it possible for geochemical techniques to detect the vertical migration of light hydrocarbon (Saunders et al., 1999; Khan et al., 2008).

Figure 3: Geochemical techniques detecting anomalous concentration of light hydrocarbon (methane-ethane) along fractures in the seepage area (Cannon et al, 2001).

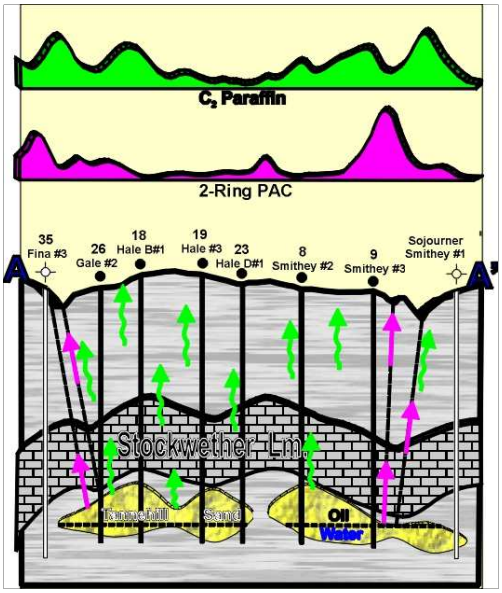

4.4 Geophysical techniques

Microbial activities can also be detected by geophysical techniques. The detection is possible due to some variation in physical properties such as change in resistivity, magnetic intensity and magnetic susceptibilities. All these variation can be associated with microbial activities (Atekwana and Slater, 2009; Atekwana and Atekwana., 2010). In the hydrocarbon seepage environment, the bio-physico chemical change is induced by different microbial activities. For instance, the secondary deposition of carbonate minerals can increase the resistivity of an initial sandstone environment from 100 to 1000 Ohm-m (Figure 4). On the other hand, a basic statistical analysis of the magnetic susceptibility measurements of 5425 drill cuttings in Venezuela showed that higher magnetic susceptibilities at the top of the sedimentary units corresponded to the reservoir and source rocks of oil-producing wells (Perez et al., 2011). Many geophysical techniques (the EM and magnetic technique in particular) can measure all these variations in physical properties mentioned above (Burger et al., 2006).

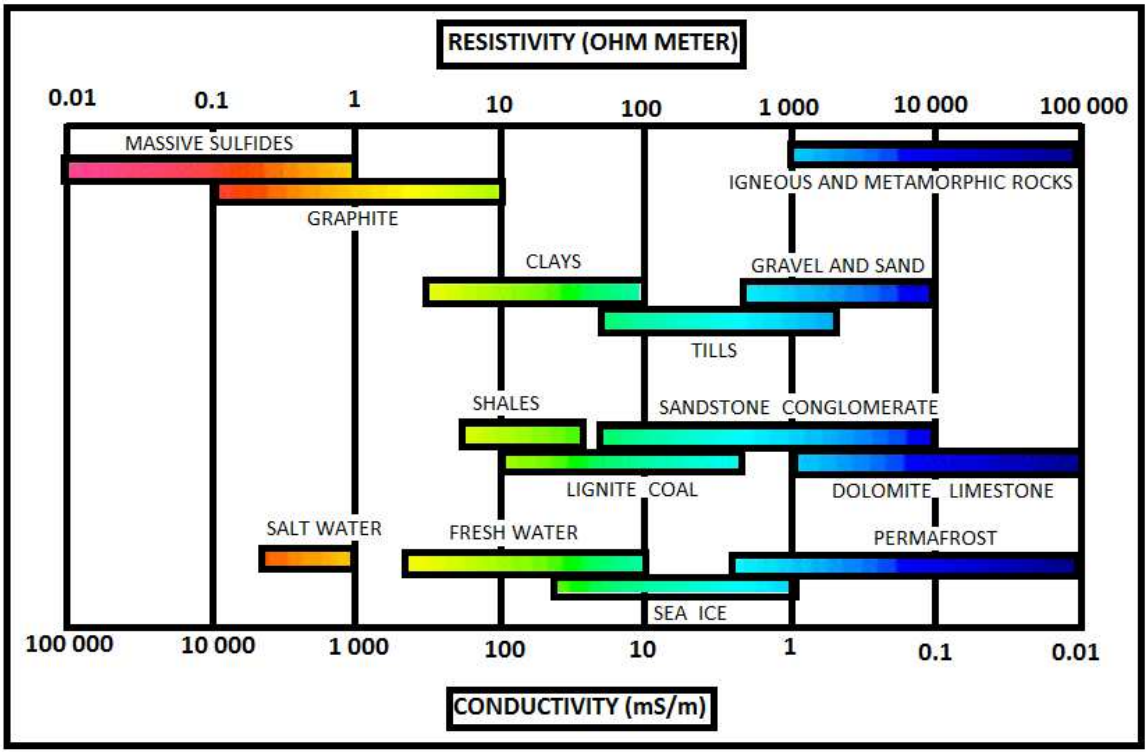

Figure 4: Range of conductivities of some common rocks. The conductivity of sandstone ranges from 4 to 15 mS/m and contrasts with that of carbonate minerals (0.01 to 1 mS/m). (Adapted from Palacky, 1987).

5 Objective

Despite the success of geophysical techniques in detecting microbial activities, it has never been applied in the detection of hydrocarbon seeps. Consequently in the present project, the EM and the magnetic techniques will be used extensively. The main objective of the study will be to explore the potential use of magnetic and electrical techniques to detect alteration zones associated with hydrocarbon seeps.

CHAPTER II

SITE GEOLOGY, TECTONIC SETTINGS AND HISTORY

1. Location

The Cement oil field straddles between Caddo and Grady counties in the State of Oklahoma (Figure 5). The name Cement was given to the town in 1902 from workers at a nearby cement mill. Gypsum that was used in the production of cement was crushed and shipped as ore (Wilson, 1976; Rackley, 2002). The Town is also known to be the center of the Hydrocarbon Induced Diagenetic Aureole (HIDA) that led to the discovery of shallow oil reserves in the Permian sequences (Al-Shaieb, 1988). The first well was drilled in 1917 and today there are more than 1500 wells drilled in the area with the cumulative oil production that averages 194 million barrels and gas production exceeding 850 bcf (Puckette et al., 2011).

The case of the Cement oil field is a good example where the change in color from reddish brown sandstone to yellowish olive gray lead to the discovery of the oil field in 1917 (Reeves, 1921). The change in color pattern had helped geologists in delineating the actual HIDA Zone. Donovan (1972) interpreted the change in color as related to the leaking of hydrocarbon reservoir. Olmstead (1975) instead, associated the change of color in local soil with the hydrocarbon productive zone. Ferguson (1977) delineated the hydrocarbon productive zone based on mapping the subsurface diagenetic pyrite. Lilburn (1981) used extensive isotope geochemistry to show that diagenetic events

are controlled by the composition and the chemistry of migrated fluid.

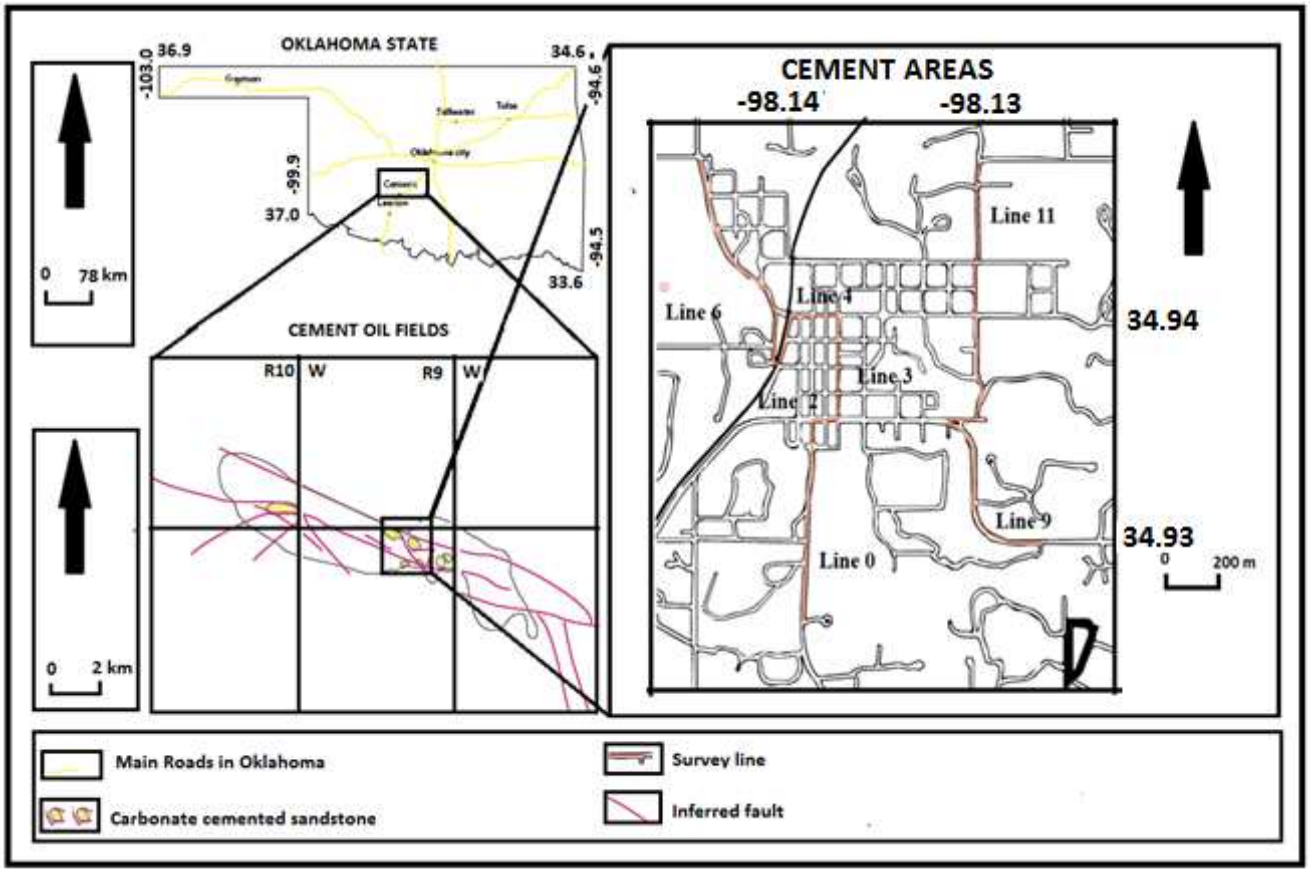

Figure 5: Location of the HIDA in the Cement oil field displaying the distribution of carbonate cemented sandstone that are closely associated with major faults Puckette et al., (2011) modified from Allen (1980). Cement areas map adapted from www.google.com.

2. Geology

The geology of the study area is described in detail by Bruce (1960). It mainly consists of Whitehorse Formation underlain by Rush Springs and Marlow Formations. These two formations are included in the 750-800 m thick Permian series that unconformably overly the Pennsylvanian groups. Permian series are believed to be deposited between Leonardian and Guadalupian tectonic events (Olmsted, 1975). The Rush Springs Formation is characterized by a composition of fine grained quartz (Bruce 1960). A microscopic analysis of the red sandstone reveals that this geological unit is composed of subangular to subrounded detrital silicate sediments that comprises mainly quartz and cherts (80%) and up to 13% of feldspars. Though microcline remain

the most abundant feldspar in the area. Fresh plagioclase are always present (Donovan, 1972). Gypsum occurs either in the veins or within a red sandstone horizons. This mode of occurrence of gypsum is common in the Marlow Formation which overlies the Rush Springs Formation (Fegurson, 1977).

In the HIDA of the Cement oil field, Rush Springs sandstone can be subdivided into two units: the altered and unaltered sandstone. The unaltered sandstone which is called red bed represents the country rock and the altered sandstone is referred to as a bleached sandstone. The color pattern of bleached sandstone horizons is believed to be directly or indirectly related to the presence of hydrocarbon (Reeves, 1921) and the concentration of carbonate cement in the country rock differentiates between zone 1, zone 2 and zone 4. When carbonate cement is absent (or almost) the red bed represents the country rock (zone 4). The Rush Springs Sandstone becomes a bleached sandstone (zone 2) when the concentration of carbonate minerals is kept to a minimum; but if the concentration of carbonate minerals increase to its maximum, the country rock is referred to as carbonate cemented sandstone (zone 1) (Figure 6). Usually the distribution of abundant carbonate cemented sandstone coincides with locations of faults (Al-Shaieb, 1988; Puckette et al., 2011)

3. Tectonic setting

Cement town is located 400 km west of the Ouachita Mountain and about 28 km east of Anadarko Basin. The sediments of most of the Permian sequences are believed to originate from Ouachita Mountain which is characterized by compressional structures (Thomas et al., 1975 & 1977). Anadarko Basin on the other hand, is believed to be characterized by the extensional structures (Gilbert, 1983 and 1987; Keller and Stephenson, 2007; Pearson et al., 2014).

A 900 m thick of Permian strata unconformably overlies a tight folded and faulted Pennsylvanian sequences (Al-Shaieb, 1988). In addition to beddings and cross beddings reported in the Cement

oil fields (Puckette et al., 2011), many sedimentary and tectonic structures occur in the Cement oil field. Most of pre Permian faults mapped in the area are oriented E-W. The north- south faults are also present. Generally the type of faults present varies from normal to reverse faults. The east-west faults tend to be associated with the occurrence of carbonate cemented sandstone. Both east-west and north south can be inferred easily from enhanced aeromagnetic maps (Figure 6).

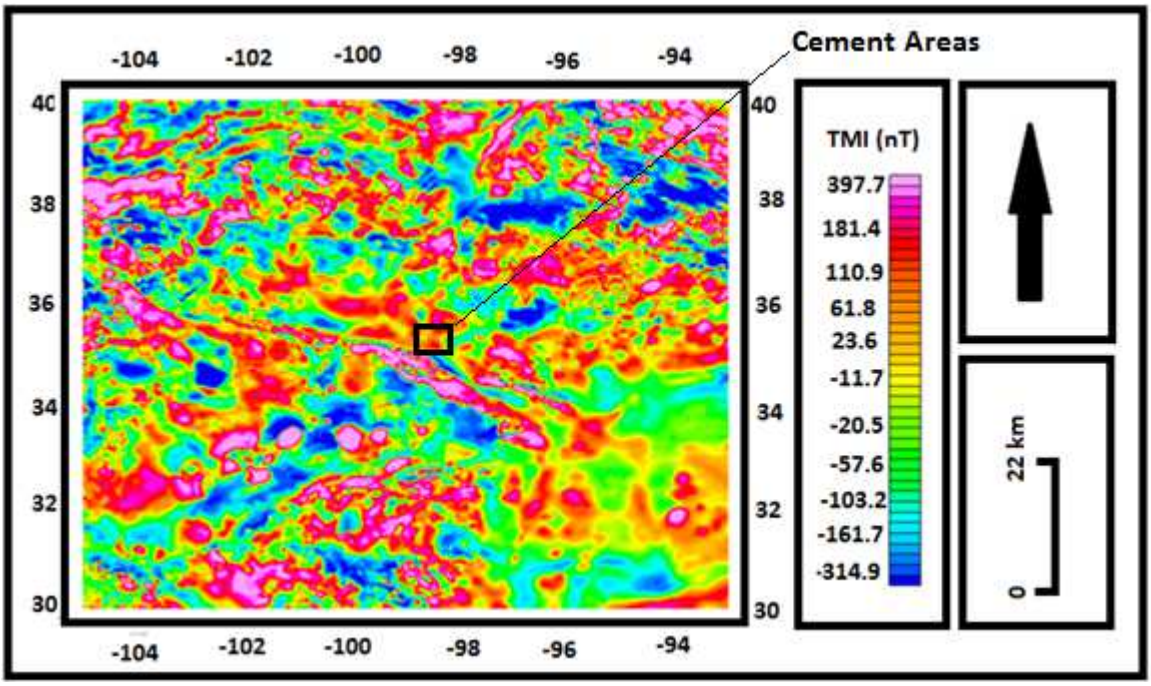

Figure 6: Magnetic anomaly map of Oklahoma krigging with aeromagnetic data from World gravity map. (http://bgi.omp.obs-mip.fr) .

4. Different Models

Several models have already been proposed to explain the occurrence of the HIDA in the Cement oil field. If the occurrence of many carbonate ridges and sulfide mineralization in the study area (Al-Shaieb, 1988) has already been associated directly or indirectly with the presence of hydrocarbon, the role played by the presence of several long term seeps in the occurrence of carbonate cemented ridges has never been elucidated.

4.1 General Model

It is clear from the generally accepted model of the HIDA of the Cement oil field (Figure 7) that the carbonate cemented sandstone (zone 1) is closely related to the major fault that acted as the conduit for oil migration from deep leaky reservoir into the Permian sequence. To some extent the lithology and the structures in the altered zone (zone 2) is strongly influenced by the presence of Zone 1. Of all the 4 zones, zone 3 is the most difficult to delineate in the field such that Fegurson had defined zone 3 in terms of pyrite content. Indeed according to this definition, any location in the zone 2 or zone 1 that contains 2% or more of pyrite can be considered as zone 3 (Fegurson, 1977).

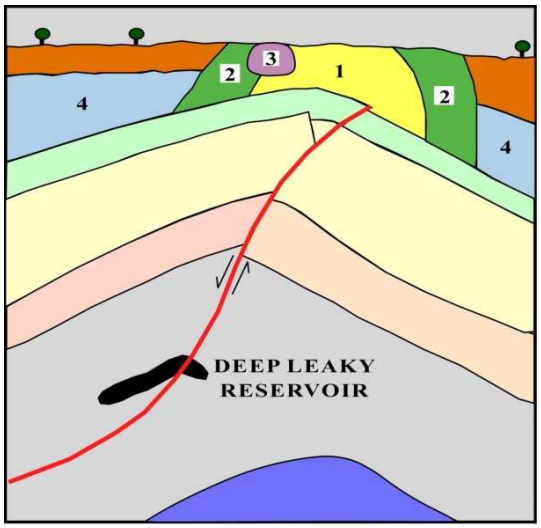

Figure 7: The general model of HIDA in the Cement oil field displaying: (1) Zone 1: carbonate cemented sandstone, (2) Zone 2: altered sandstone,(3) Zone 3: sulfide Zone and (4) Zone 4: the unaltered sandstone. (Puckette et al., 2011).

4. 2 Schumacher Model

The simplified model of Schumacher (1996) summarizes all the models that have been proposed for the HIDAS of the Cement oil field so far (Donovan, 1972; Allen, 1980; Al-Shaieb, 1988; Price, 1986). The Schumacher Model can be subdivided into 5 phases (Figure 8):

1. **Vertical migration of hydrocarbon (light hydrocarbon)**

In the seepage areas, light hydrocarbon (methane up to butane) migrated vertically up to the earth surface through network of fractures or discontinuities.

2. Aerobic condition of methane by microbial activities

As light hydrocarbons were migrating upward, they were consumed by oxidizing bacteria.

3. Anaerobic condition and production of bicarbonate

The methane consumption by oxidizing bacteria enhanced the decrease in oxygen that resulted into anaerobic conditions, consequently into the production of reduced sulfur.

4. Combination of iron with Sulfur

The combination of sulfur with iron already present in the local environment lead to the formation of iron sulfides and iron oxides.

5. Calcite precipitation

Calcite precipitation was enhanced by the change in PH due to continuous production of bicarbonate.

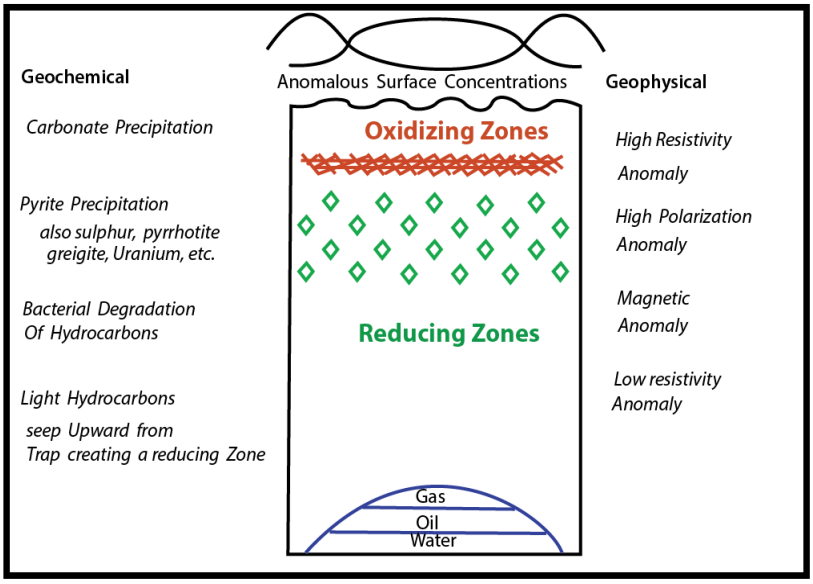

Figure 8: The Schumacher Model of the HIDA displaying the sulfide zone characterized by high polarization anomaly and low resistivity (Schumacher, 1996).

4. 3 Drake Model

Unlike the Schumacher (1996) model where the formation of pyrite results from the diffusion of hydrogen sulfide into iron rich horizons, in the Drake Model (Figure 9) pyrite precipitation results from the chemical of at least two aqueous solutions. Pyrite precipitation is explained by chemical reactions between deeper water relatively poor in sulphate but with higher concentration of carbonate ions and the surface rich water (in granitic environment) characterized by very low concentration of bicarbonate. The chemical reaction between these two types of fluids can occur in fractures or microfractures where they are catalyzed by appropriate bacterial activities (Drake et al., 2014).

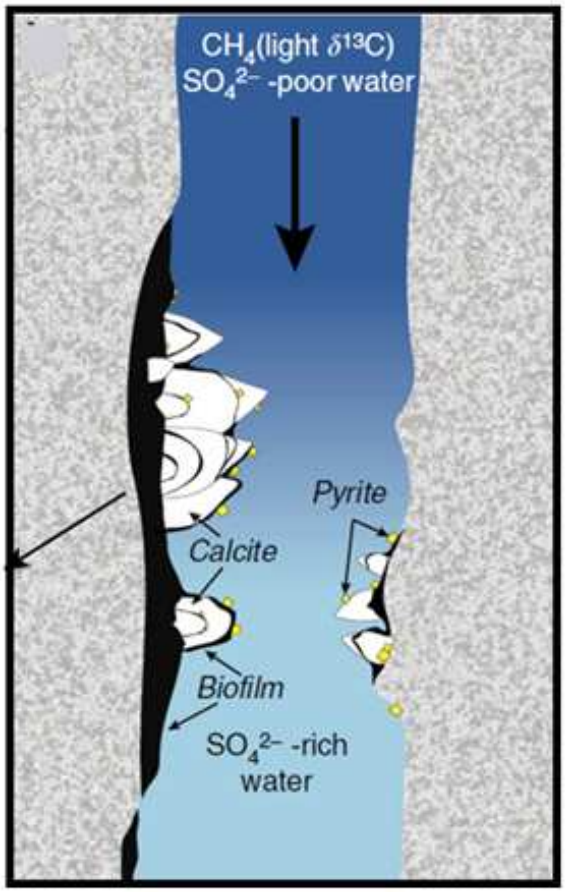

Figure 9: Precipitation of pyrite and formation of calcite from chemical reaction between surface and deep water. The surface water is poor in sulfate and rich in carbonate. The deep water is rich in sulfate and poor carbonate. chemical reactions occur in presence of sulphate reducing bacteria in microfracture of about 800 micron (Drake et al., 2014).

CHAPTER III

METHODOLOGY

1. Introduction

All the details about the electromagnetic (EM) (Figure 9) and magnetic techniques that were used in the present survey are described extensively in Burger et al., (2006) and Telford et al., (1976). Only a brief summary of the principles is presented in this chapter. In any case EM surveying is mainly based on the second (Faraday law) and fourth Maxwell equation (Ampere-Maxwell) (Marescot, 2015[i]; Turnbull, 2013).

$$\nabla \times H = \frac{\partial D}{\partial t} + J \qquad (1)$$

The EM technique consists of generating a time varying magnetic field by moving a source AC current in a transmitter. The primary field generated in the transmitter induces eddy currents in a potential conductor buried in the subsurface. By circulating in the subsurface the eddy currents generate a secondary magnetic field that can be detected by a receiver coil. In fact the receiver detects the resultant of both primary EM and the secondary EM (Burger et al., 2006). Many electromagnetic equipment have the capability of converting the magnetic intensity into conductivity. Precisely, the Geonic EM31 and EM 34 have been chosen in the present survey because they are capable of converting magnetic intensity into conductivity.

The magnetic survey on the other hand, consists of investigating the variability of the rock magnetization or small perturbations of the earth's magnetic field.

Interpretation of magnetic data depends on variation of the earth magnetic field (Ihsan et al., 1970; Telford et al., 1976). Magnetic field at any point on earth can be fully defined by its total intensity and its direction consequently, a variety of geophysical equipment can be used to measure that change in magnetic intensity (Burger et al., 2006).

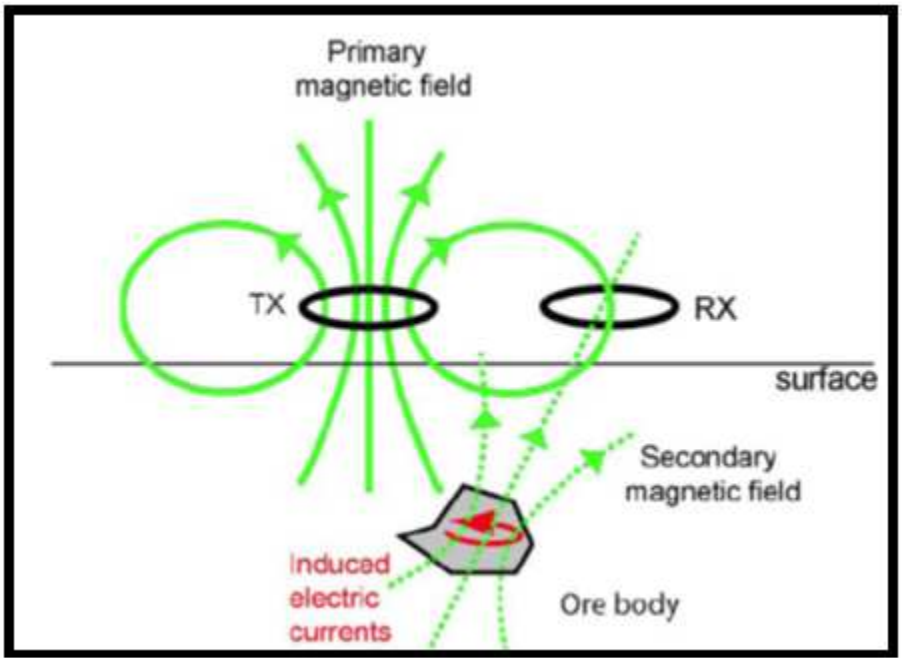

Figure 10: Principle of Electromagnetic Survey based on application of the 3rd Maxwell Equation (Faraday law), 4th Maxwell equation (Ampere Law) (unknown source).*

Both electromagnetic and magnetic surveys have already recorded successes in environmental and engineering applications. Atekwana et al. (2004) successfully used EM techniques to map variations in conductivity resulting from microbial degradation of oil at a decommissioned refinery in Michigan. In addition, recently it has been shown that magnetic susceptibility is a viable tool for detecting zones of oil degradation by microorganisms (Rijal et al., 2010; Mewafy et al., 2011; Atekwana et al., 2014).

2. Electromagnetic Survey with EM31

During the present survey data were acquired in the discreet mode. The EM31-MK2 was set at both inphase and quadrature mode. Both vertical and horizontal mode were chosen and the

equipment was operated in the manual mode. The GPS was not attached to the equipment instead the interval between way points was kept at about 5 m spacing. At the end of the survey, 899 measurements were obtained. Most magnetic readings and their respective locations are described in the Appendix 1.

After plotting the inphase and the bulk conductivity of the 9 profiles (Figure 11), abrupt negative spikes of inphase components within a profile were interpreted as resulting either from the presence of a buried metallic conductor or from minerals such as pyrite, pyrrotite, etc. Values of bulk conductivities in the sulfide zone were expected to be relatively higher as compared to those of unaltered Rush Springs sandstone Formation.

3. Electromagnetic survey with EM 34

Two loops of configurations, horizontal dipole (HD) and vertical dipole (VD) were used during the EM survey with EM 34. Consequently, two types of data were recorded at each station. Measurements were taken with a 10 m cable separating the receiver and the transmitter. Unlike the survey with EM31, the spacing interval between stations was maintained at 10 m apart. Given that the survey with EM 34 was performed only on line 0, line 6 and line11, only 439 measurements were obtained at the end of survey.

4. Magnetic Survey

All the total magnetic intensities data were acquired using Geometrics G858 cesium vapor magnetometer in the simple survey. Data were acquired using 5m station spacing along the profiles in a unidirectional mode. A total of 1708 measurements were obtained at the end of the magnetic survey. Magnetic cleanliness was observed: objects such as belt buckles, metal eyeglasses, clipboards, watches, pens, and the wallets coins were kept away from the sensor which was maintained at 1.50 m above the ground throughout the survey.

The diurnal corrections applied on the base line (line 0) revealed that the magnetic intensity was increasing by 0.0205 nT/s. This rate was found to be negligible. The difference in topography between the highest and the lowest point in the study area was found to be 40 m. This difference in topography was considered negligible and it is the reason why elevation correction could not be performed however, all the data were IGRF corrected.

5. Magnetic susceptibility

The color pattern of local soil at each station was recorded simultaneously while taking geophysical reading. At the end of the survey, about 10 soil samples representing different types of soils in the area were collected. The magnetic susceptibilities were measured at HBRC lab using MS2 with MS2B probes. The soil density was computed while reading the magnetic susceptibility of the soil samples using analytical and precision balance (Vibra HT series).

6. Source of interference

Many sources of interference occur throughout the study area consequently there was need to study them in detail by establishing with accuracy how they affect the data collected in the field. The main sources of interference consists of railroad tracks, buried pipelines, metallic fences and residential buildings.

In addition to the proximity of sources of interference, the configuration of the coil (especially for the data collected with EM34), the direction of the survey line (parallel or perpendicular to the sources) affected differently both the EM and the magnetic surveys. In most cases, there were warning messages to alert about the type of interference. However, it is important to bear in mind that normally, EM 31 and G858 Cesium magnetometer are designed to detect most of the sources of interference as mentioned above such that even without warnings posters (Geometrics, 2001; Geomatrix, 2015[1]), the 2 equipment would have detected successfully most of the source of

[1] Year the website has been accessed

interference described above. On the other hand, considerable effort was made to avoid cultural noise. However, some sources of interference could not be avoided as data had to be collected continuously along well planned survey lines. In any case, at the end of the survey, signatures from different sources of interference were evaluated accordingly.

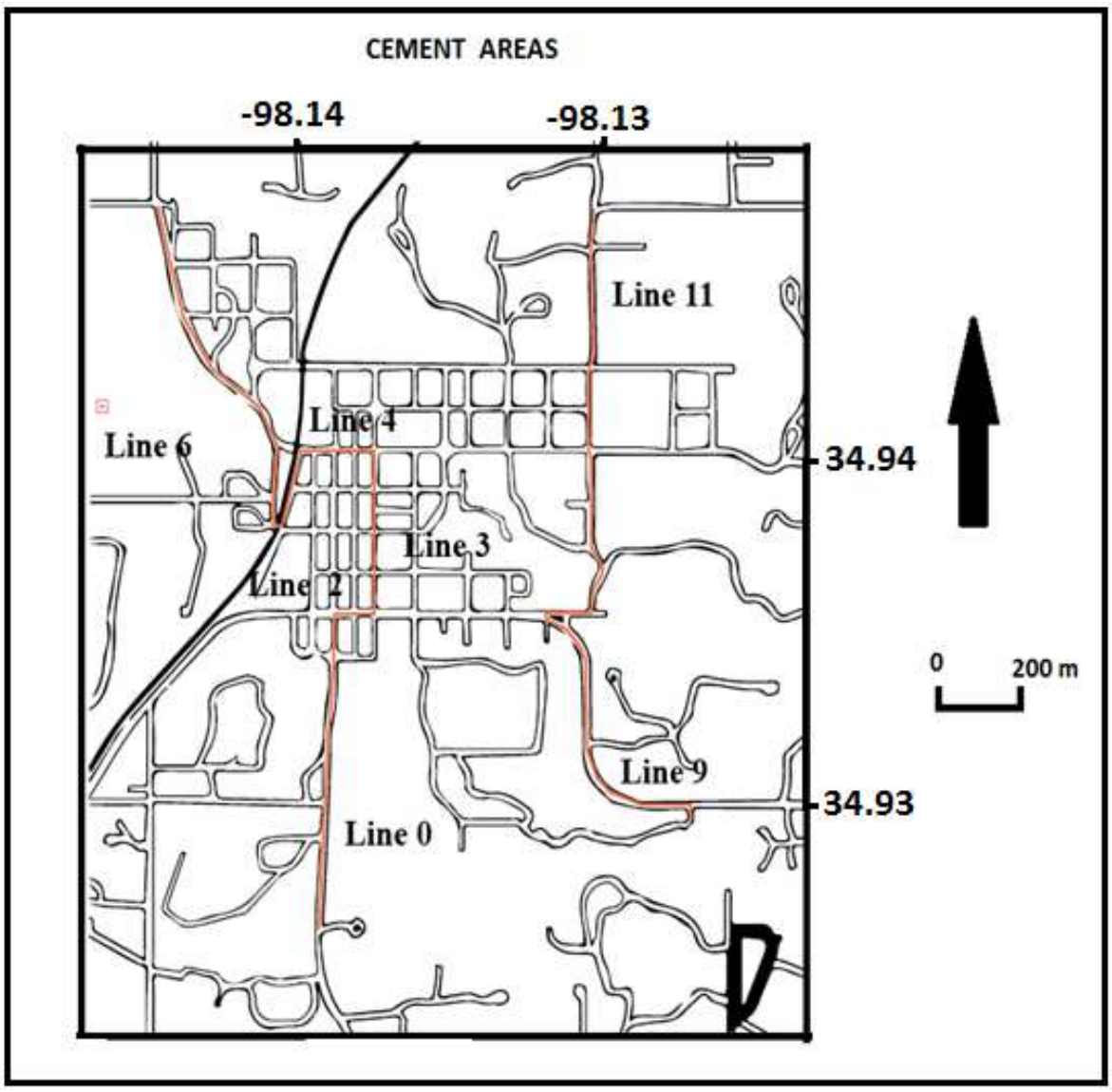

Figure 11: Cement Town displaying the 9 Survey lines (in red). Map adapted from the Google map (www.google.com/maps).

CHAPTER IV

RESULTS

1. Effect of the railroad tracks

A north-south rail road track cross cuts the study area in the west. Though the rail track intersects both the survey lines 5 and 6, the origin of line 6 is the closest to the rail road track. In fact the most significant peak associated with rail road track was recorded in the vicinity of the station 0 m (Figure 12). Generally, the readings of bulk conductivity on stations located on distances less than 15 m away from the rail road tracks seemed to be affected. With the EM 34 electromagnetic survey it was found that both HD and VD are affected in the vicinity of the rail road track. However, the VD seems to be more affected. These results suggest that the easiest way to correct the effects of the rail roads will be by discarding all data recorded on stations located on a distance less than 20 m away from the rail road track (Duran, 2014).

2. Effect of buried cables and pipelines

Several warning posters indicate the location of buried cables and pipelines in the study area. Figure 13 describes the signatures of the EM and magnetic intensity along the line 11 where some pipelines or electrical cables were buried. In any case a detailed study of men made interference shows that in general, during the electromagnetic survey with EM 31, both the quadrature and the inphase conductivities tend to decrease abruptly in the vicinity of buried electrical cables.

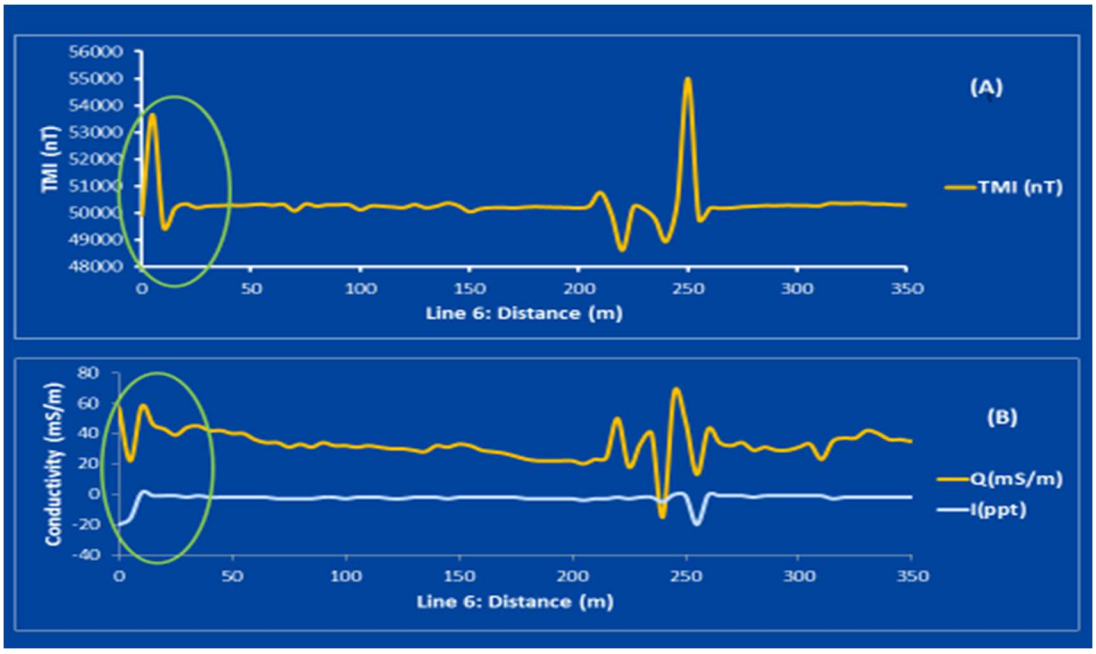

,.

Figure 12: Effects of the railroad track (circled region) along profile Oklahoma Avenue (line 6) on (a) Magnetic and (b) EM Survey.

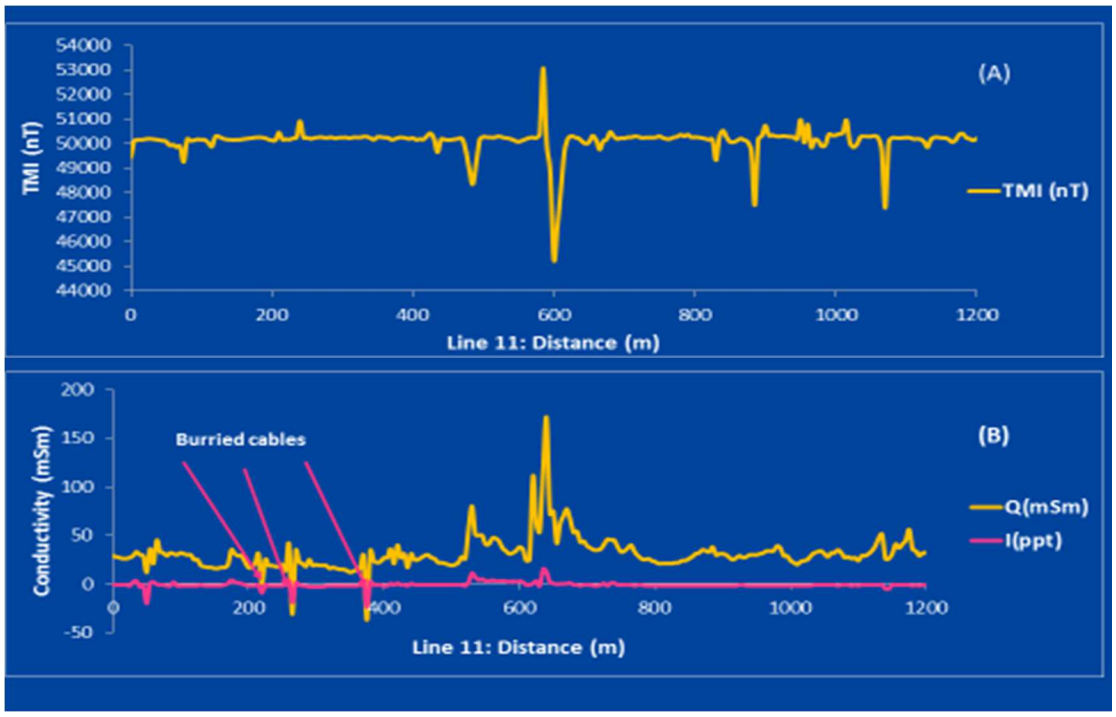

Figure 13: Effects of the Buried cables along profile Oklahoma Avenue (line 11 on (a) Magnetic and (b) EM Survey.

Given that most significant interference recorded with EM 31 occurs when the equipment was directly above the source of interference (Figure 13), the effect of buried pipe can be easily filtered by discarding all the data collected within 15 m away from the source of interference.

3. Effect of powerlines

A network of powerlines covers the whole study area. Though the height of power lines was not measured in the field, it is reasonable to believe that the minimum height of 5.5 m as fixed by the National Electrical code for powerlines or less was respected in the study area (Timothy, 2015). Almost all the survey lines run parallel to the powerlines.

During the electromagnetic survey with EM34, the validity of the data collected was dictated by the relationship between the height of the power line and the intercoil spacing. Given that the intercoil spacing was fixed at 10 m, data had to be recorded at least 13 m away from the power line (1.5 m away far from the source:15 m) (Duran, 2014). On the other hand, with EM 31 which is characterized by the coil spacing of 3.6 m, the minimum distance from the powerlines was kept at 5.5 m (Figure 13).

4. Effect of metallic fences

Generally for metallic fences higher than 2m, the interference was expected to be negligible beyond a distance of 20 m (Duran, 2014). However, the analysis of data collected in the vicinity of metallic fences on line 0 and line 11 respectively, describes the general characteristic of EM and magnetic signature that can be expected when a profile is affected by the interference of metallic fences (Figure 14). It is clear that in the vicinity of a cultural source of noise, EM data recorded with EM 31 tend to give the same value of the bulk conductivity throughout the areas of interference such that on the profiles they appear as horizontal lines. To filter data from the effect of metallic fences (of 2m high), anomalous data recorded in the distance less than 20 m away from the fences were considered invalid and ignored.

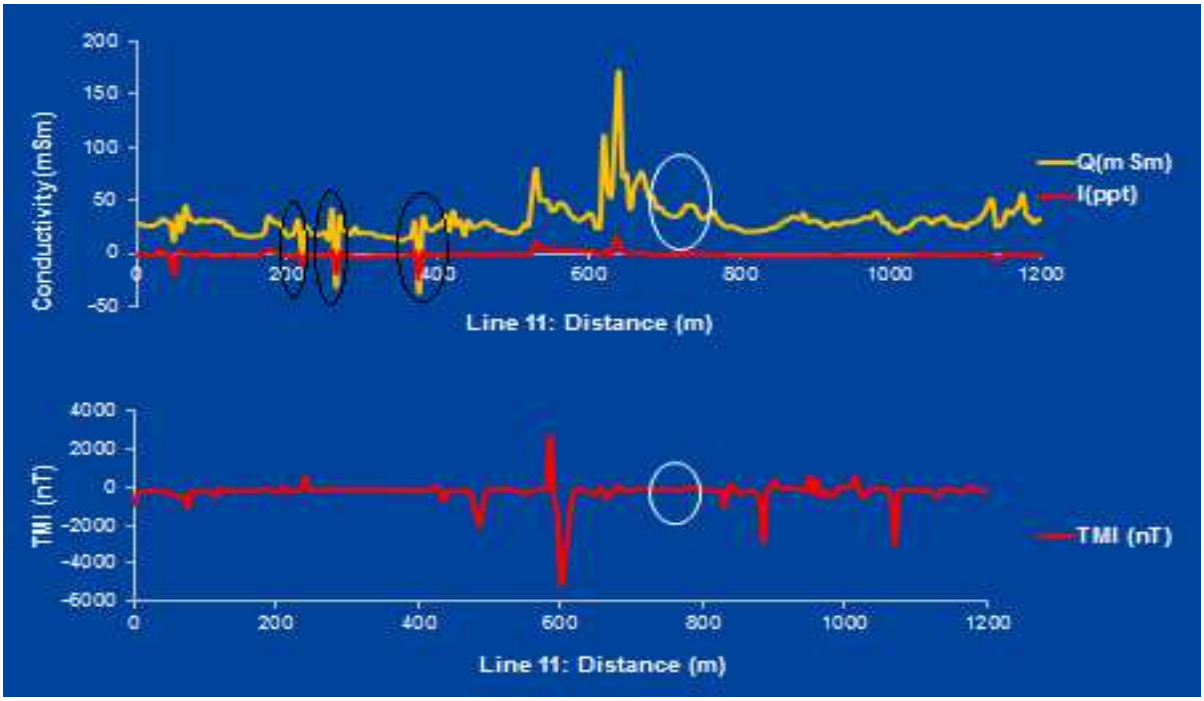

Figure 14: Black circles represent the effects of buried pipes along Line 11 (H Avenue) on EM Survey while white circles represent the effect of metallic fence on both EM and magnetic survey.

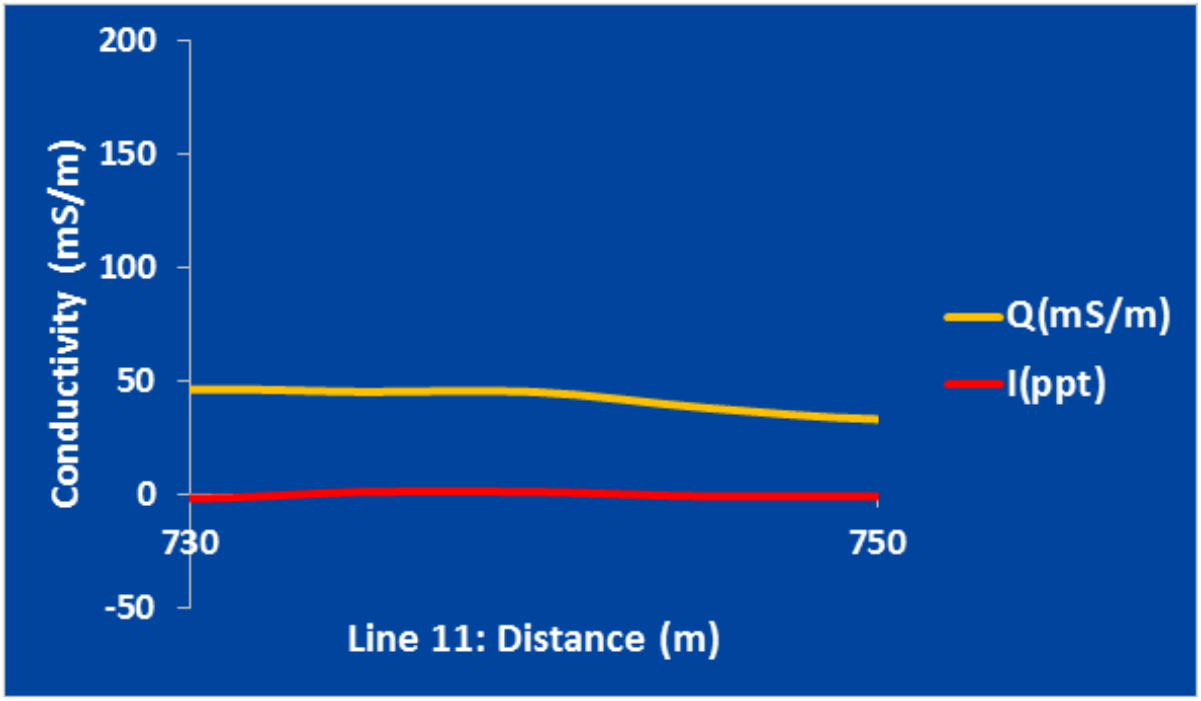

Figure 15: Effect of Metallic fences along line 0 on (a) EM and (b) Magnetic Surveys.

5. Analysis of different survey lines

The characteristic signature of buried cables, and buried pipe are easy to identify on a geophysical profile. In most cases they are different from those recorded at the contact zone between zone 1 and zone 2. The difference between these two types of signature is so significant that even by keeping the signature of men made interferences on the 9 different profiles, data recorded could still be interpreted successfully.

5.1 Line 0

On the line 0 (Figure 16), the highest bulk conductivity (204 mS/m) has been recorded 3 times with EM31 consecutively at station 840 m, 845 m and 850 m. The station 850 is only 15 m away from station 865 m where the highest magnetic field (53030.08 nT) has been recorded. This station coincides with the contact between carbonate cemented sandstone and altered Rush Springs sandstone (Figure 17). The highest horizontal dipole (HD) bulk conductivity reading along the line 0 was recorded with EM 34 at the station 770 m. On the other hand, the highest vertical dipole (VD) (311 mS/m) occurs 120 m away from the station 750. Higher values of the VD readings were also recorded in the anomalous interval (820-840 m) where contact between carbonate cemented sandstone and Rush Springs sandstone has been inferred (Figure 16). The 20 m of discrepancy between the VD peak at 750 m and the HD peak at 770 m can be justified by the fact that the plane of discontinuity is dipping. Precisely the dip direction has been used to compute (20° SW) using the Equation (1) below. σ is dip angle, H_{vd} H_{hd} are the depth of penetration for vertical and horizontal dipoles, and Xhd, Yhd represent stations where the higher HD and VD have been recorded within a reasonable interval.

$$tan\sigma = \frac{H_{VD} - H_{HD}}{X_{HD} - Y_{VD}} \qquad (1)$$

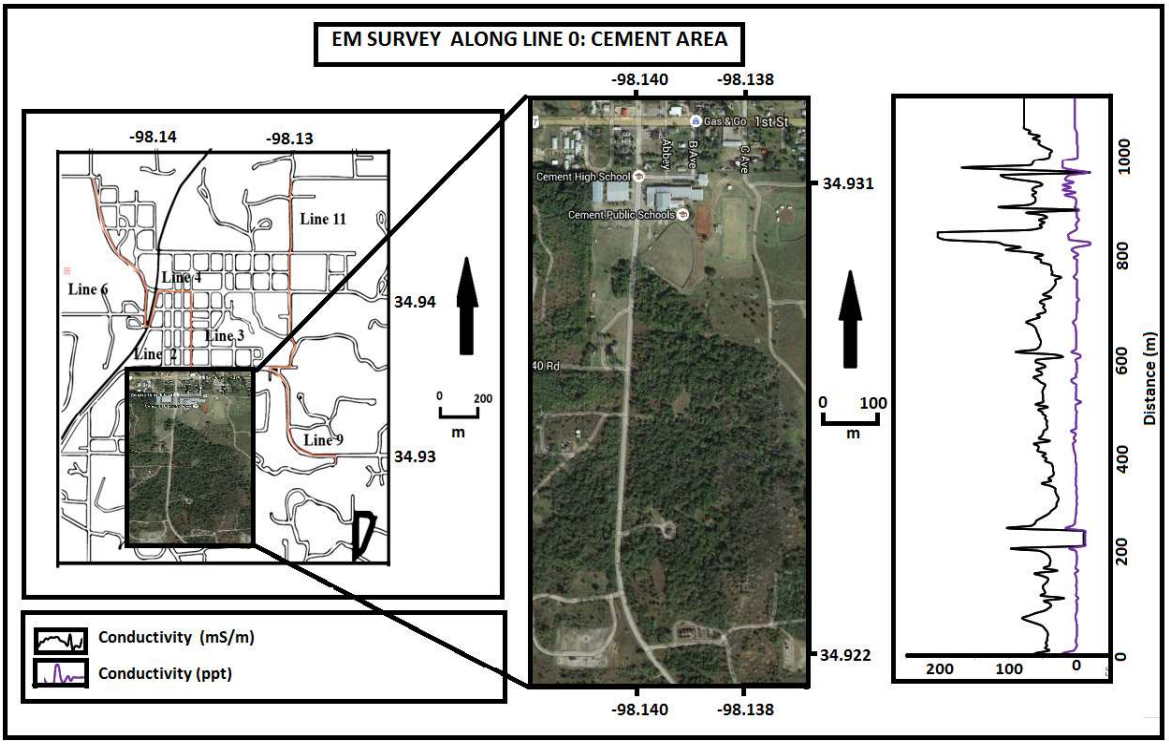

Figure 16: Electromagnetic and magnetic surveys with EM 31, EM 34 and G858 Cesium magnetometer along the Line 0. The signature of both bulk conductivity and total magnetic intensity are complex in the interval 800-1065 m where the highest magnetic intensity was also recorded. Map Adapted from google map.

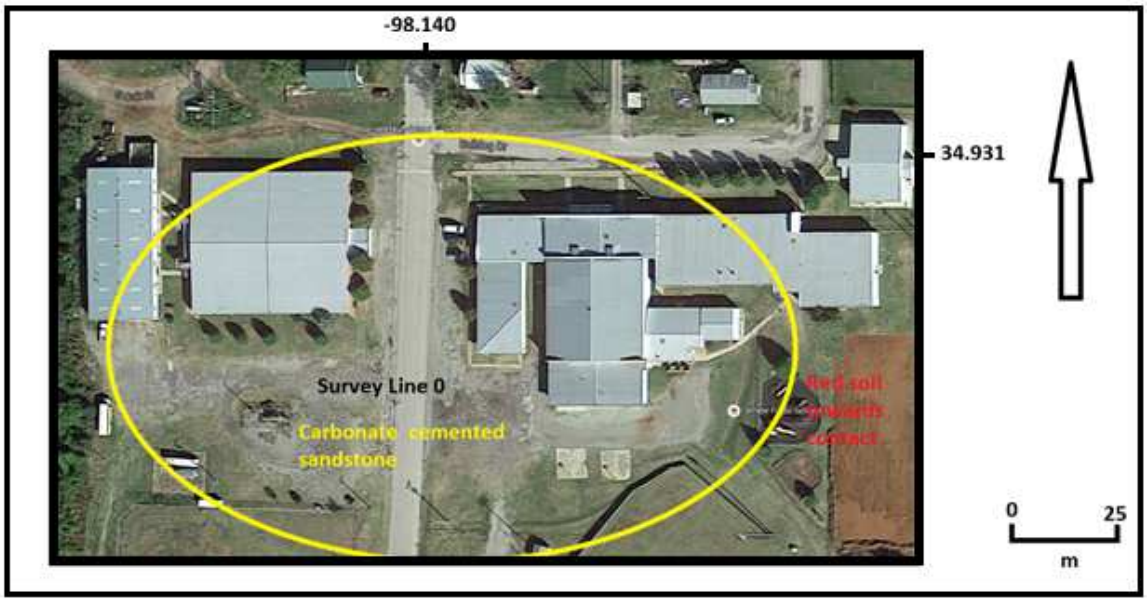

Figure 17: The larger scale of the map on the figure 15 displaying cream grey outcrop that was interpreted as carbonate cemented sandstone along the Line 0. Adapted from maps.google.com.

5.2 Line 2

On line 2 (Appendix 2), the minimum bulk conductivity recorded with EM31 in the interval 40 to 60 m displays more the characteristic of a buried cable and consequently does not yield any significance in the study of HIDA of the Cement oil field. However, the lowest magnetic intensity recorded at the beginning of the line is difficult to interpret. It coincides with the occurrence of a filling station.

5. 3 Line 3

On survey line 3, the signature of the bulk conductivity is more complex in the interval from the station 200 to 410 m (Figure 18). The end of the line coincides with the contact between carbonate cemented sandstone ridge and the altered Rush Springs sandstone. Though the highest peak 204 (mS/m) can be traced at the station 370 m, the anomalous zone starts from 360 m. All the stations within the interval 200-410 m are characterized by a relative higher bulk of conductivity. This interval can be subdivided into two sections: the first section from 225 to 270 m and the second from 345 to 390 m. The boundaries between zone 2, zone 3 and zone 1 can be tentatively extrapolated from the profile 3 (Figure 19).

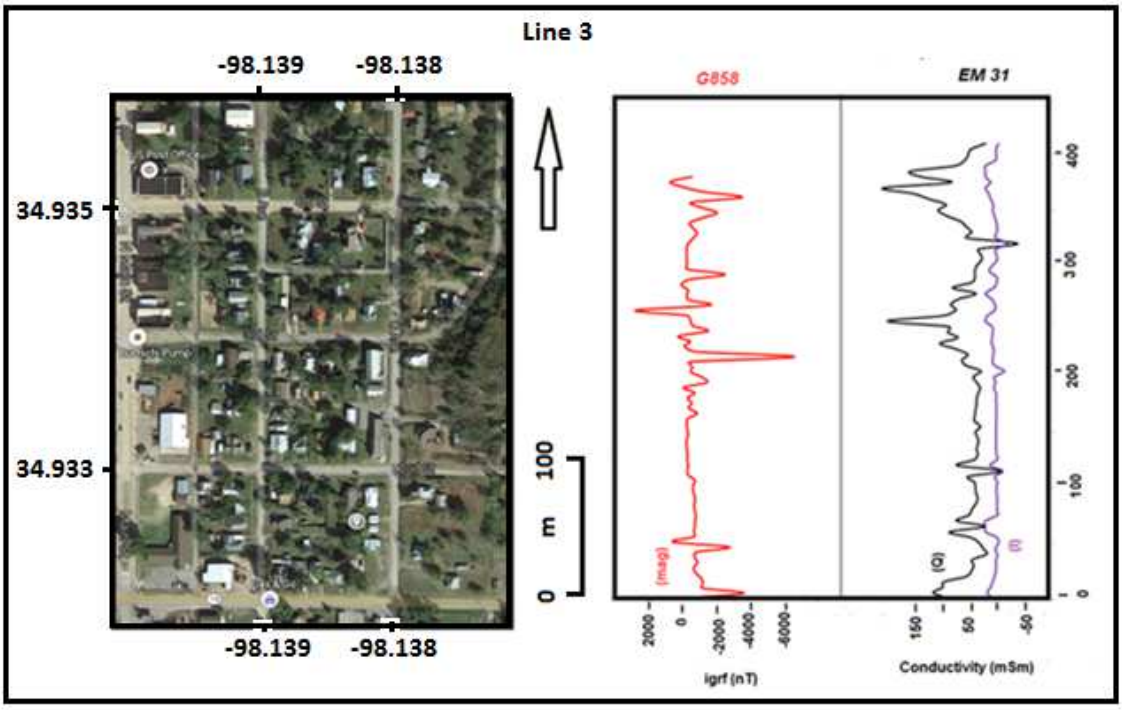

Figure 18: Electromagnetic and magnetic surveys with EM 31 and G858 cesium magnetometer respectively along the Line 3. Adapted from google map..

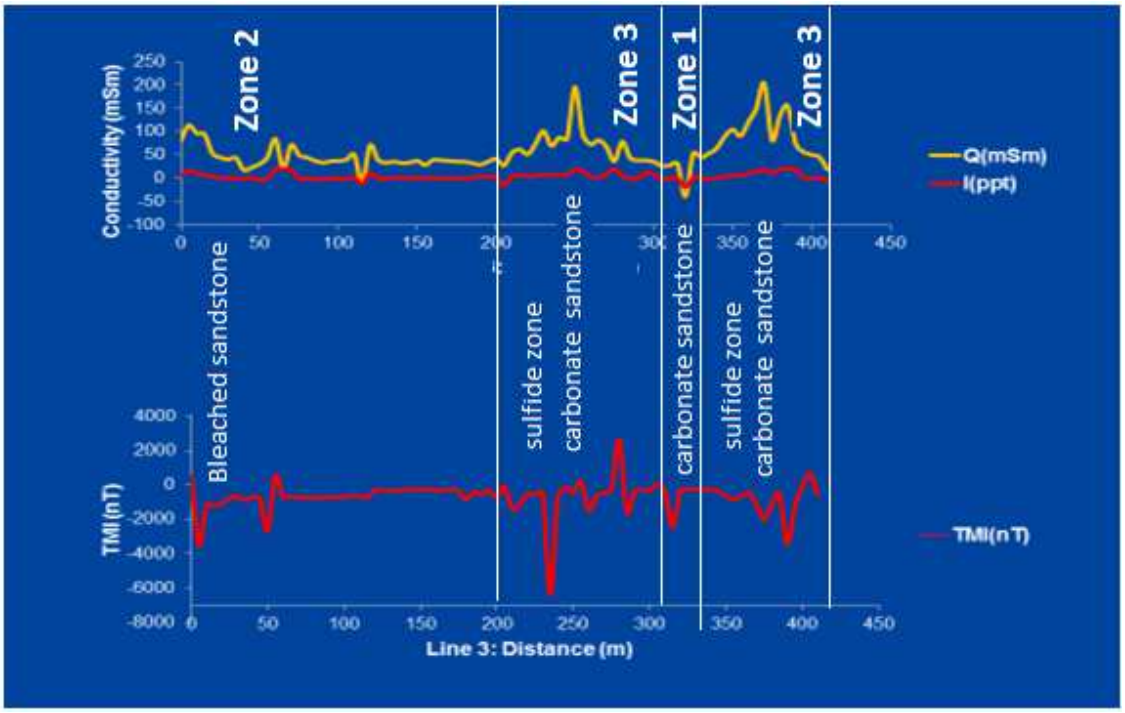

Figure 19: EM and Magnetic Profiles along the Line 3. The characteristic signature at the contact between carbonate cemented sandstone and bleached sandstone.

5. 4 Line 4

The highest bulk conductivity (79 mS/m) occurs at station 170 on survey line 4 while the highest magnetic intensities were recorded consecutively at station 190 and 195 m. Station 195 is located almost at the end of the survey line 4, at about 50 m away from the contact between light olive grayish soil and reddish soil (Annex 2: Figure 32). Most likely the 3000 m square of reddish soil at the end of the survey line 4 results from the alteration of greenish gray outcrops. This type of alteration is very common in the carbonate cemented sandstone environment. In any case the lowest bulk conductivity (-59 mS/m) of the line has been recorded 120 m away from the origin.

5. 5 Line 5

On the line 5 (Appendix 3) the highest bulk conductivity (80 mS/m) was recorded with EM31 at the station 115 m. This station is located 5 m away south of the station 110 where the highest magnetic intensity of the line (51460.26 nT) has also been recorded. The bulk conductivity displays the characteristic of buried cables. The occurrence of piles of metallic poles outside a warehouse on the road side might have contributed as a source of interference. However, it is important to mention the occurrence of a greenish gray outcrop some 15 meters away from the metallic poles.

5. 6. Line 6

Except for some anomalous readings recorded in the vicinity of the station 0 m, higher values of bulk conductivity and magnetic intensity were recorded in the 200-300 m interval (Figure 20). As mentioned earlier on, the anomaly in the vicinity of the 0 m was associated to the presence of the rail road track. In any case the highest value of both bulk conductivity (67 mS/m) and magnetic intensity (55002.852 nT) occur in the interval 200-300 m which coincides with the presence of a greenish gray outcrop (carbonate cemented sandstone). The signature of bulk conductivity as

recorded with EM31 displays some complexity within the same anomalous interval. With the EM34, the highest bulk conductivity VD and HD were recorded towards the end of the line. The fact that the boundary between altered (zone 2) and unaltered sandstone (zone 4) cuts across towards the end of this line, opens another possibility to the interpretation of this signature (Figure 21).

Figure 20: Electromagnetic and magnetic survey with EM 31, EM 34 and G858 cesium magnetometer along Line 6. Adapted from google map.

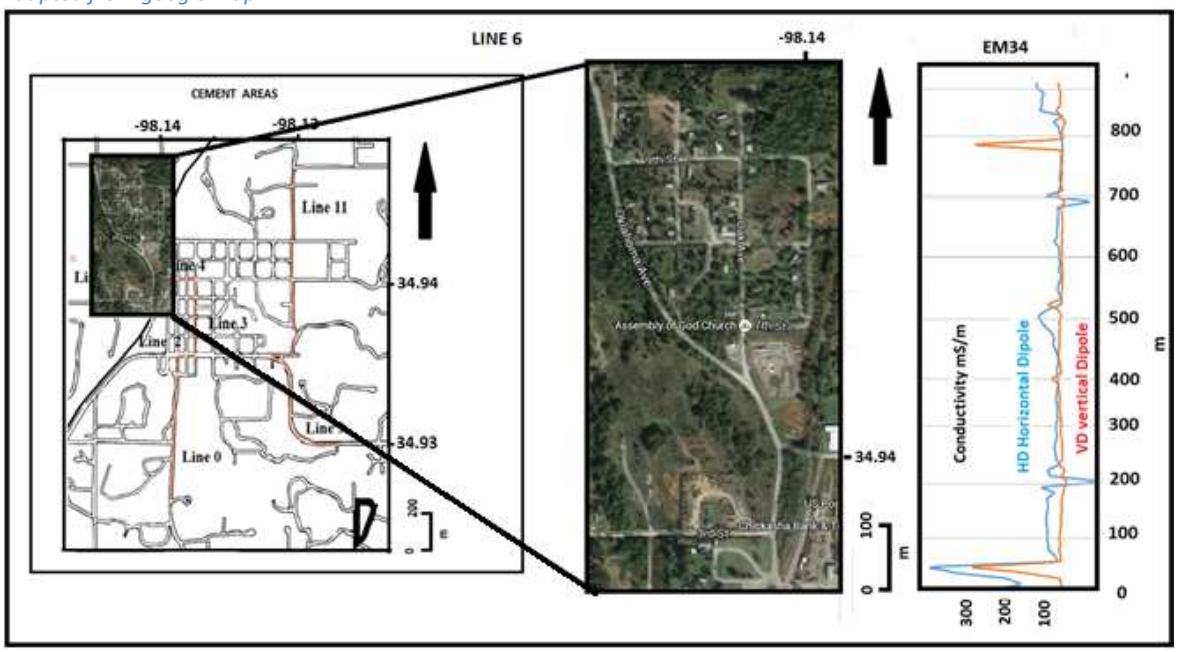

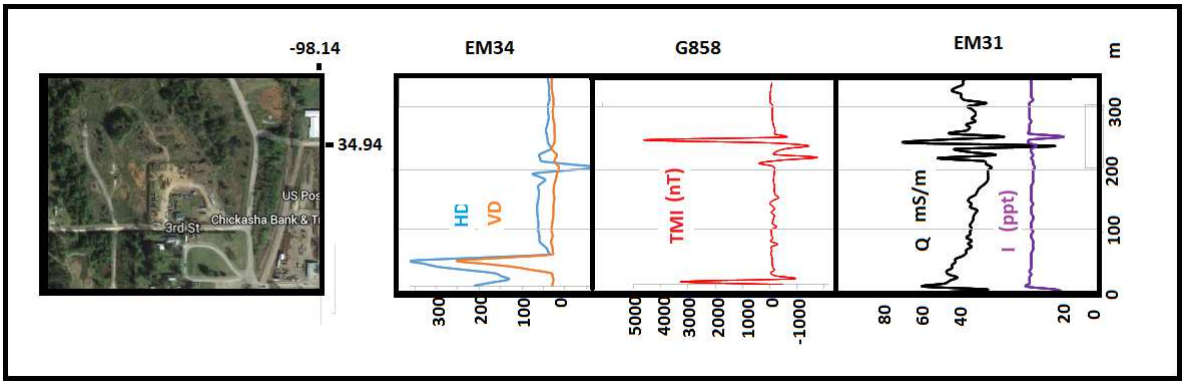

Figure 21: EM and Magnetic Profiles along Oklahoma Avenue (Line 6).

5.7 Line 7

Both the inphase (I) and bulk conductivities (Q) reach their maximum values respectively 3 ppt and 33 mS/m at station 35 on the line 7 (Annex 5). Then, simultaneously decrease down to lower values at station 45 m. However, the lowest bulk conductivity has been recorded at station 20 m. Except for the highest total magnetic intensity (52216.93 nT) that has been recorded at the end of the line, stations with higher total magnetic intensity have been recorded in the 30-50 m interval. The maximum magnetic intensity (50497.25 nT) occurs at station 35. This value drops at its lowest (49524.53nT) at station 40 m. Though this line has been selected because it was believed to cut across the HIDA boundary, the anomalous reading seems to be associated with the sharp contact between carbonate cemented sandstone (zone 1) and Rush Springs Sandstone (zone 2).

5. 8 Line 9

On the line 9 (Figure 22) the highest magnetic intensity (55315.87 nT) has been recorded in the red soil at the station 560. It is the highest magnetic intensity recorded throughout the survey area. The lowest magnetic intensity (42174.32 nT) occurs just 15 m away from the station 560 (at the station 585). Two outcrops of carbonate cemented sandstone have been mapped 120 m away from the survey line 9 from station 0 to 300. The occurrence of these two carbonate cemented sandstone outcrops have already been described extensively in the previous reports by Allen (1980). Though the contact between the bleached sandstone (zone 2) and carbonate cemented sandstone (zone 1) was not delineated accurately in the present survey, it is reasonable to believe that the boundary is not far from the survey line. In any case it is important to bear in mind that there are many small magnetic anomalies that tend to be associated with ephemeral drainages (Figure 23).

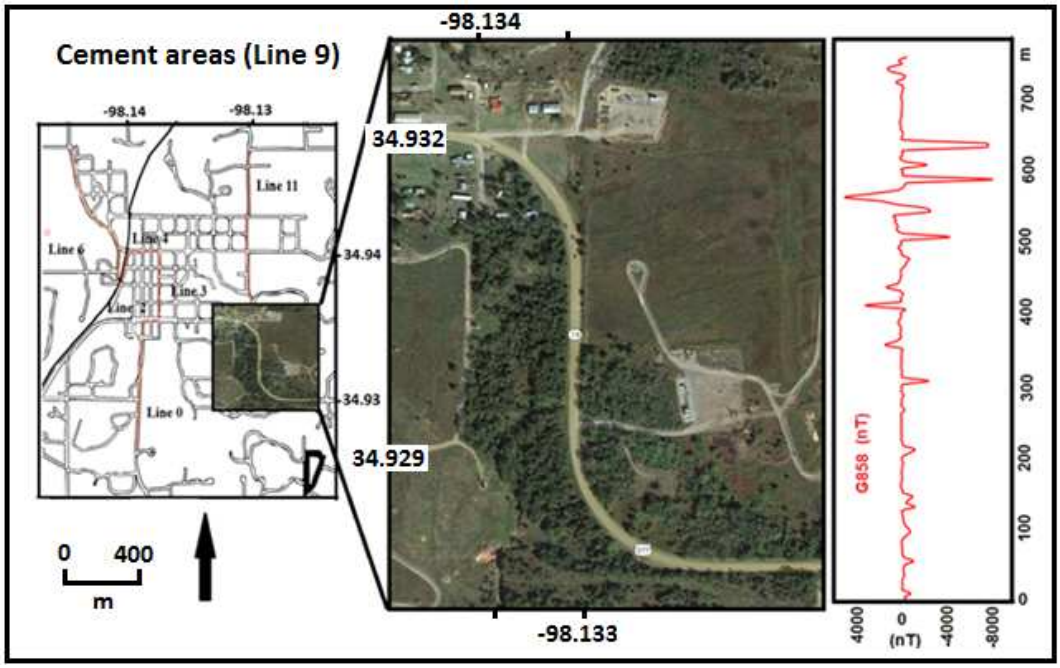

Figure 22: Electromagnetic and magnetic surveys with EM 31 and G858 cesium magnetometer along the Line 9. Adapted from google map.

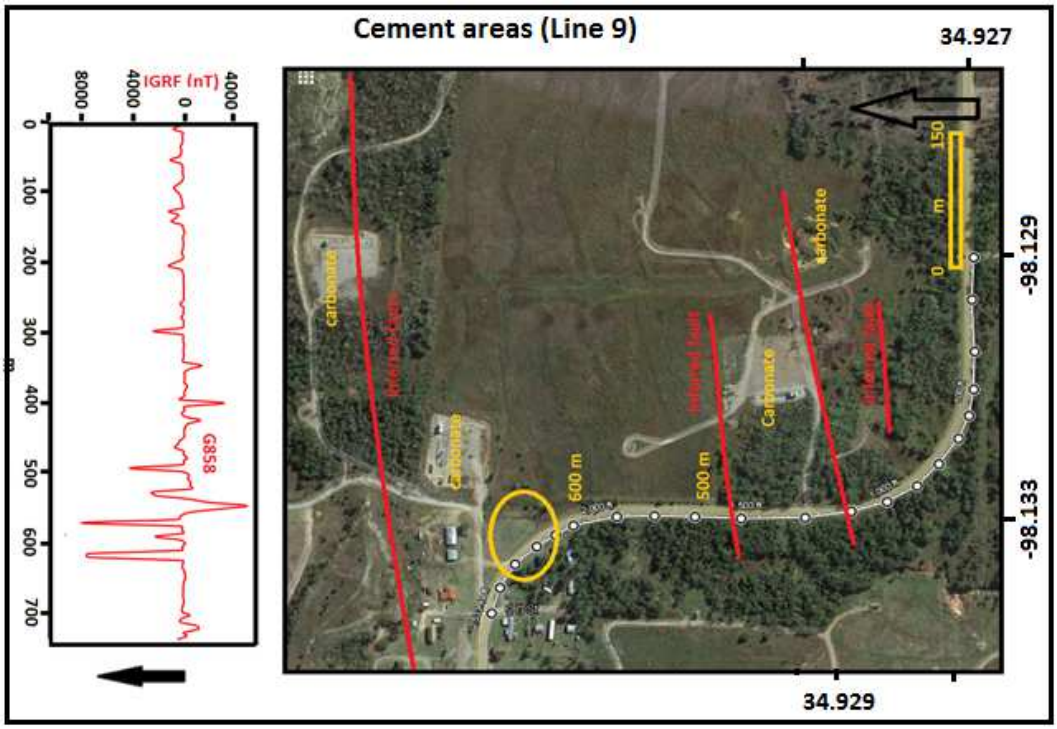

Figure 23: Electromagnetic and magnetic surveys with EM 31 and G858 cesium magnetometer along the Line 9. Adapted from google map.

5. 9 Line 11

On the line 11 (Figure 24), the highest bulk conductivity (171 mS/m) has been recorded with EM31 at the station 640. Indeed on the satellite image, the interval from the station 550 to 700 corresponds to a different tone in color that has been mapped as carbonate cemented sandstone in previous studies (Allen, 1980) (Figure 25). Even higher bulk conductivity VD (175 mS/m) recorded with EM34 occurs within this interval. The negative peak at the station 375 is associated with buried pipeline. On the other hand, the average magnetic intensity was found to be 49961.06 nT with the highest reading recorded at the station 585 in the light brown soil. The lowest magnetic (45297.05 nT) was read 15 m away towards the south (station 600 m).

5. 10 Geophysical signature between zone 2 and 1

In the field, carbonate cemented sandstone outcrops in areas characterized by higher topography. On satellite images, these areas can be easily identified by a characteristic light greenish gray tones (Figure 25). The contact between the carbonate cemented sandstone and bleached sandstone can also be detected by a significant increase in the magnetic intensity and in bulk conductivity from zone 1 (z1) to zone 2 (z2) or vice versa. In most cases zone 1 is adjacent to zone 2 (unless zone 3 is present). Though the presence of z3 is difficult to be detected in the field, on EM profiles it is recognized by an abrupt increase in the bulk conductivity (Table 1). The increase in the bulk conductivity can also be visible in the variation of magnetic intensity from z1 to z2 (Table 2).

Figure 24: Electromagnetic and magnetic surveys with EM 31 and G858 cesium magnetometer along the Line 11. Adapted from google map.

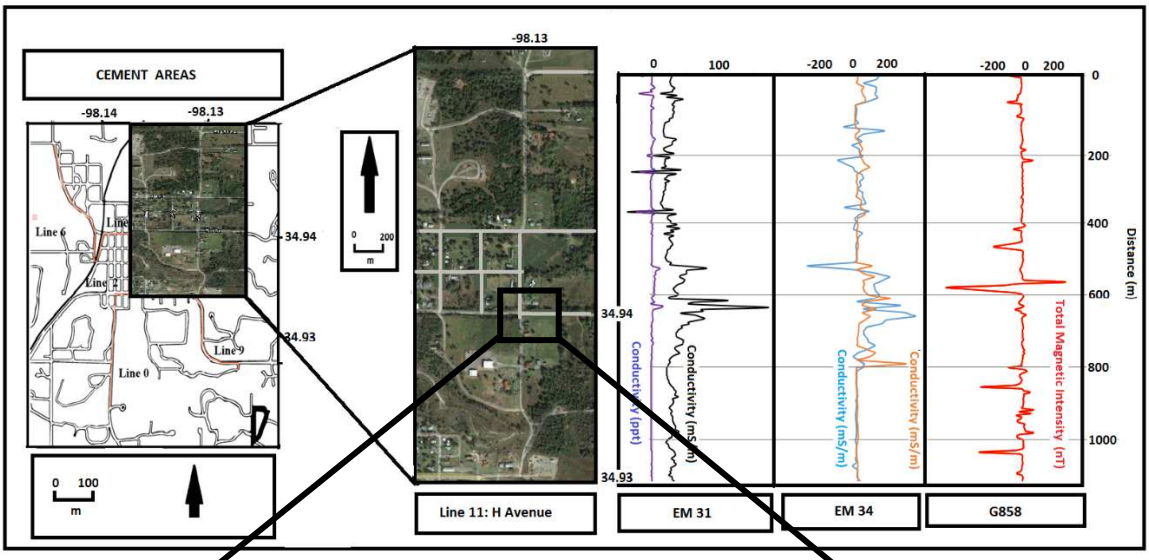

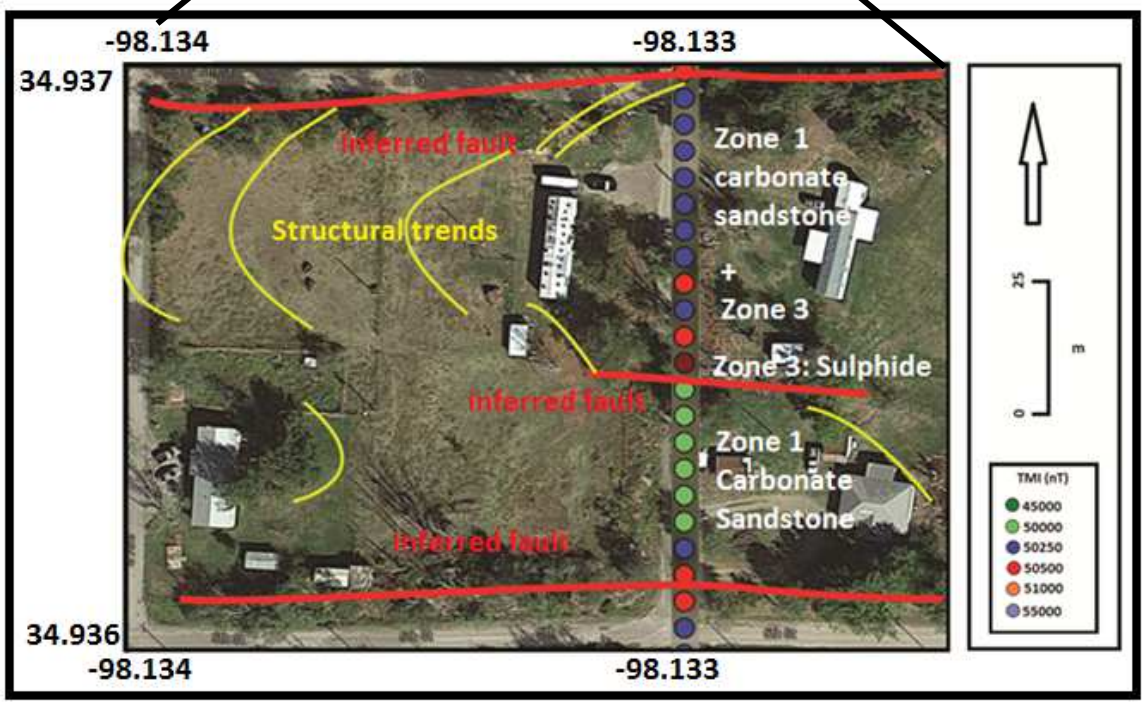

Figure 25: Interpretation from the magnetic surveys with G858 cesium magnetometer along the Line 11 from 550-650 m. Map adapted from google map.

Table 1: Variation of magnetic intensity of the 9 profiles in the intervals where there are higher probability to cross the boundary between carbonate cemented sandstone (Zone 1) and the altered sandstone (Zone 2).

Line	Interval (m)	Location (m)	Zones Boundary Z_1/Z_2	Background Mag Strength (nT)	Maximum Mag Strength (nT)	increment %
0	800-1065	865	Z1/Z2	50267	50535.32	0.53
2	70-120	95	Z1/Z2?	49854	50312.59	0.92
3	200-350	280	Z1/Z2	49664.	53019.67	6.76
4	170-200	200	Z1/Z2?	50078.5	51104.05	2.04
5	100-200	110	Z1/Z2	50012.76	51460.26	2.89
6	200-300	250	Z1/Z2	50212.37	55002.85	9.54
7	30-50	50	Z1/Z2?	50218.55	52216.92	3.98
9	100-300	195	Z1/Z2	50257.18	55315.87	10.07
11	450-650	585	Z1/Z2	50314	53091.15	5.52

If the variation of the magnetic conductivity at the boundary between z1 to z2 ranges from 2 to 10.07%, the range of variation of the bulk conductivity as recorded with EM31 can reach 450 % consequently, the increase of the bulk conductivity at the boundary between z1 and z2 will be easier to detect especially when zone 3 is present.

Table 2: Variation of electromagnetic bulk conductivity (Q) of the 9 profiles in the intervals where there is higher probability to cross the boundary between the carbonate cemented sandstone (Zone 1) and the altered sandstone (Zone 2).

Line	Interval (m)	Location (m)	Zone Boundary Z_1/Z_2	Background Conductivity (mSm)	Max (EM31) Conductivity (mSm)	Increment %
0	800-1065	840	Z1/Z2	35	204	482.86
2	70-120	35	Z1/Z2?	78	163	108.97
3	200-400	370	Z1/Z2	38	204	436.84
4	170-200	175	Z1/Z2?	38	79	107.89
5	100-200	115	Z1/Z2	29	80	175.86
6	200-300	245	Z1/Z2	25	67	168
7	30-50	35	Z1/Z2?	26	33	26.92
11	450-650	640	Z1/Z2	31	171	451.61

On the other hand, the fact that anomalous bulk conductivities have been recorded with EM34 (Table 3), suggests that the contact between zone 1 and zone 2 can been traced down even in the deeper horizons.

Table 3: Variation of electromagnetic bulk conductivity (VD) of profiles 0, 6 and 11 in the intervals where there is higher probability to cut across the boundary between the carbonate cemented sandstone (Zone 1) and the altered sandstone (Zone 2).

Line	Interval (m)	Location (m)	Zone Boundary Z_1/Z_2	Background Conductivity (mSm)	Max (EM34) Conductivity (mSm)	Increment %
0	700-900	770	Z1/Z2	42	294	600
6	750-900	780	Z1/Z2	44	245	456.82
11	600-850	790	Z1/Z2	44	320	627.27

5. 11 Magnetic susceptibility

As far as the distribution of soil types and their respective colors are concerned, 65 % of local soil color patterns were found to be light brown while 25% are brick red. The rest of the soil types vary from light olive gray to cream light brown (which is the general characteristic of the bleached sandstone). The density of the soil samples collected in the area varies from 1.99 to 2.3 g/cm^3. The general characteristic of magnetic susceptibility of different types of soils is described in Table 4. The difference in magnetic susceptibility of various soil sample can be explained by the progressive accumulation of detrital minerals such as magnetite that are relatively denser and more resistant to weathering (Breiner, 1973)

The Figure 26 displays the distribution of the soil samples collected in the study area. Unlike the sample 5B1, sample 6A1 was collected far from the boundary between zone 4 and zone 2, therefore it represents the country rock (zone 4). Sample 3 A1, on the other hand, represents zone 1 (carbonate cemented sandstone). Sample 1A1, on the other hand was collected at the boundary between zone 1 and a weathered zone characterized by red soil. While the rest of the samples (A1, 1A2, 2A1, 1B1) are scattered within the alteration zone (zone 2).

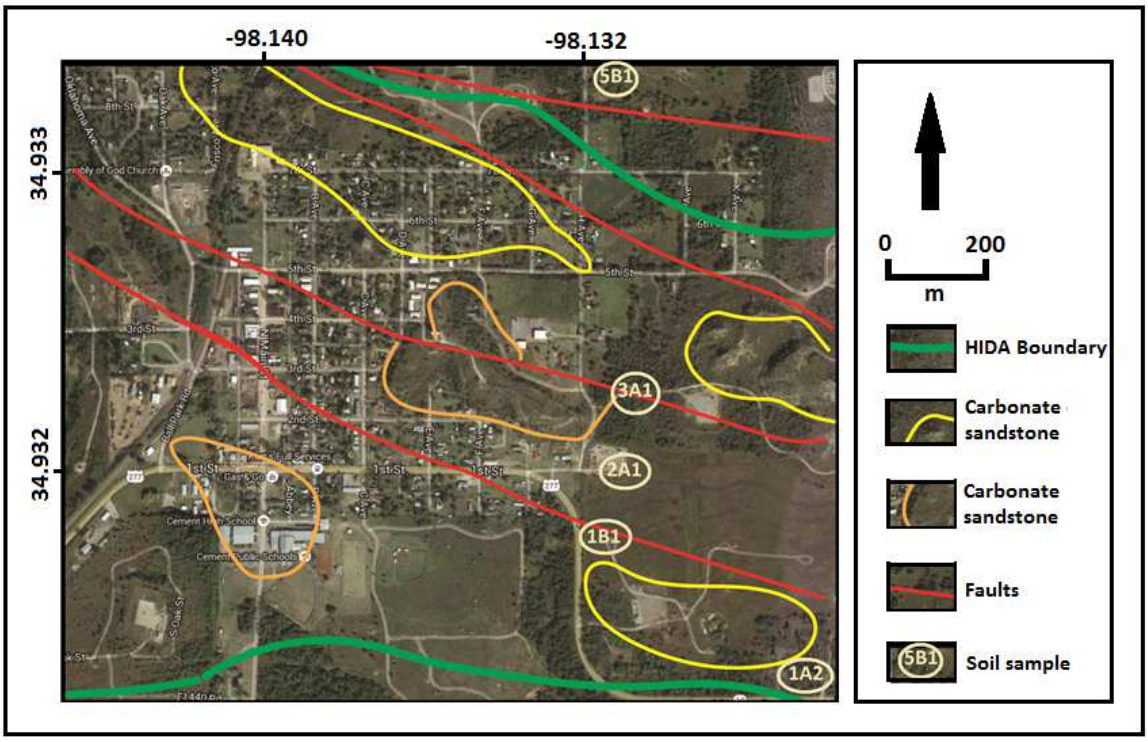

Figure 26: Location of soil sample throughout the study area. Map adapted from google map. See Table 4.

The results of magnetic susceptibility in Table 6 suggests that the magnetic susceptibility of soil samples is the lowest in the carbonate cemented sandstone (zone 1). This can be explained by the fact that the deposition of carbonate minerals corresponds with the decrease in the magnetic susceptibility. Compared to the soil sample collected in the country rock (6A1), the magnetic susceptibility in the alteration zone was found to be relatively higher (Figure 27).

Table 4: Magnetic susceptibility of soil samples.

Samples	Full	MS (SI)	Color Code
6A1	12.9056	0.5	10R 4/6
1A	14.7838	2.4	10R 4/6
1A2	14.4752	0.8	10R 3/4
2A1	13.3566	1.1	10R 2/2
3A1	13.3492	0	5GY 3/2
1B1	15.0112	2	10R 2/2
5B1	14.0702	1.2	10R 3/4

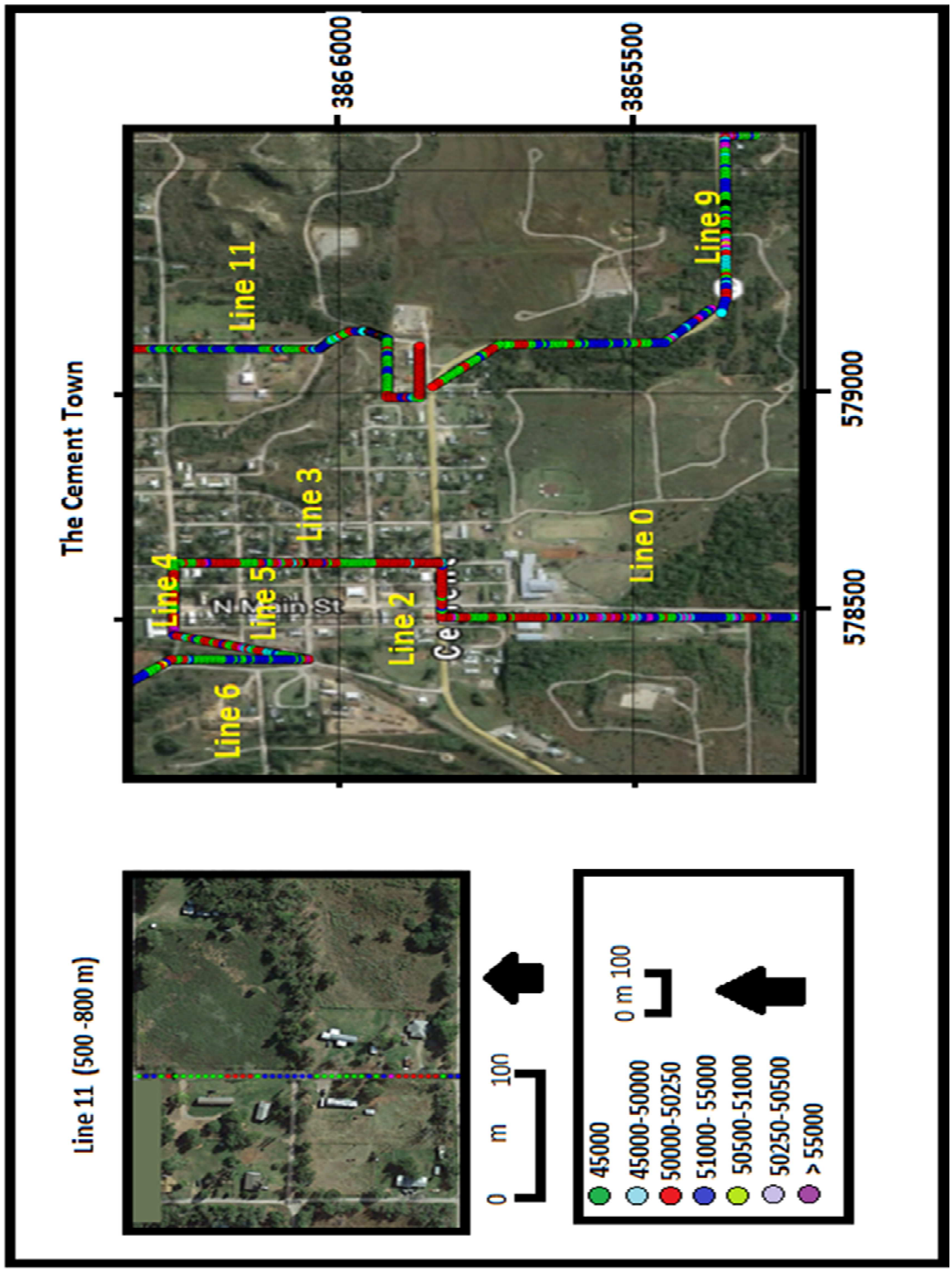

Figure 27: Map of total magnetic intensity in the study area Including all 9 profiles. Adapted from google map.

.

CHAPTER V

DISCUSSION

1 Introduction

The analysis of both magnetic intensity and bulk conductivity profiles suggests that there is increase of the two geophysical parameters at the boundary between zone 2 (altered sandstone) and zone 1 (carbonate cemented sandstone) (Figure 28 and 29); yet generally, the variation of the bulk conductivity from sandstone (1000 mS/m) to carbonate minerals (limestone) would be expected to decrease at least by 10% (Palacky, 1987).

This situation raises some questions: what is the significance of anomalous readings on the boundary between altered sandstone and carbonate cemented sandstone zone? Or more precisely, do the anomalous readings in the bulk conductivity recorded at the contact between 2 zones relate to the presence of pyrite along fault walls or planes of weaknesses? To provide answers to these two questions there is need to develop a comprehensive model of HIDA that will take into consideration the present geophysical data, as well as the condition of precipitation of major minerals that have already been reported in the area. Whether minerals developed along fault walls or not the main question remains: can the geophysical techniques detect successfully long term hydrocarbon seeps?

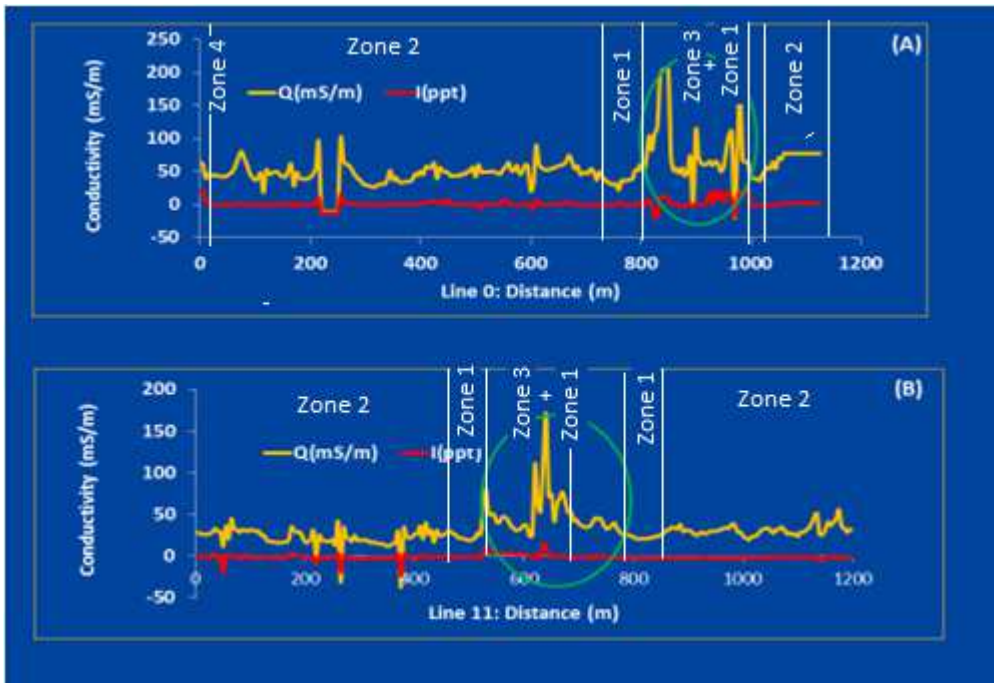

Figure 28: Characteristic of the bulk conductivity signature towards the contact between carbonate cemented sandstone and bleached sandstone on the profile (a) line 0 (b) line (11).

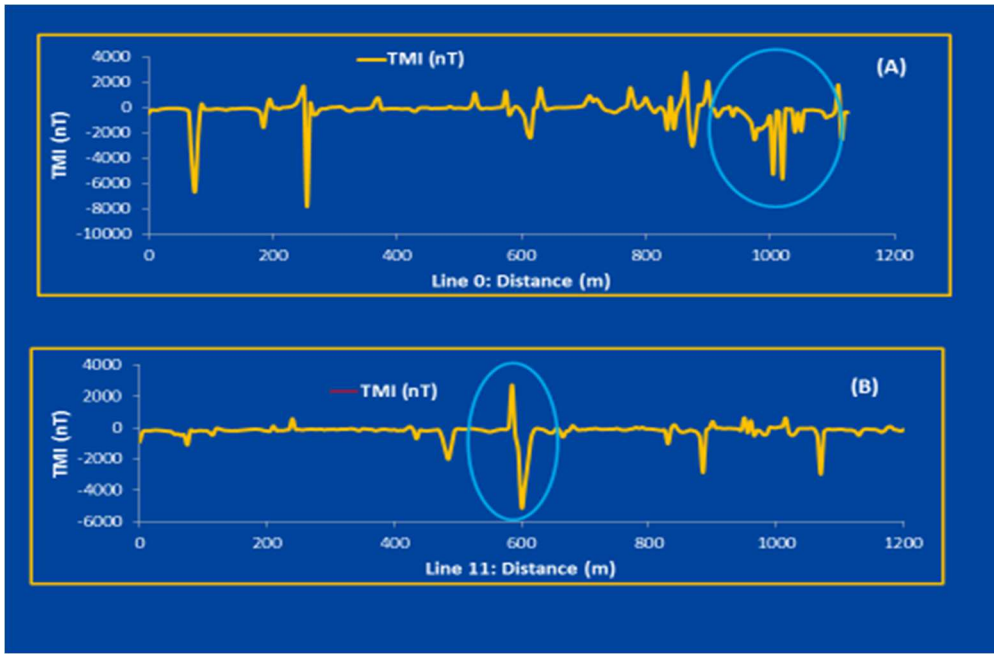

Figure 29: The characteristic signatures of the total magnetic intensity at the contact between carbonate sandstone and bleached sandstone for line 0 and line 11.

To detect successfully long term hydrocarbon seeps, an efficient technique must be able at least to discriminate between two consecutives zones of the 4 (Allen, 1980, Al-Shaieb, 1988, Fegurson, 1977). Additionally, if the boundary between the zone 2 (altered sandstone) and the zone 4 (unaltered sandstone) can be detected efficiently, then the Whole HIDA region would be delineated successfully.

On the other hand, bearing in mind that the sulfide zone is adjacent to both bleached sandstone and carbonate cemented zone (Figure 6), by singling out the sulfide zone, it is possible to delineate the boundary of both the carbonate cemented sandstone and zone 2. Hence, there is need to delineate with geophysical techniques both the pyrite zone and the carbonate cemented sandstone zone. There is also need to analyze closely the characteristic of the geophysical signature at the boundary between altered and unaltered sandstone.

2 Altered and unaltered sandstone boundary zone

Bearing in mind that the boundary between the altered (bleached sandstone) and unaltered sandstone (country rock) is gradational, some difficulties to delineate the two zones in the field have to be expected. Consequently, portions of geophysical profiles that cross cut the boundary between the bleached sandstone (zone 2) and the country rock (zone 4) will be discussed in term of probability. Indeed the 4 portions of the survey lines 0, 6, 7 and 11 where there was higher probability of crossing the zone2/zone 4 boundary are described in the Table 8 and Table 9 respectively for the EM and magnetic technique.

Table 5: Variation of total magnetic intensity of in the 4 intervals where there is higher probability to cross the boundary between the altered sandstone (Zone 2) and the unaltered sandstone (Zone 4).

Line #	Interval (m)	Location (m)	Zone Boundary Z_2/Z_4	Background Mag Strength (nT)	Max mag Strength (nT)	Increment %
0	150-250	175	Z2/Z4	49879.79	48754.48;	-3.2
6	650-750		Z2/Z4			
7	0-50	50	Z2/Z4	50218.55	52216.92	-1.9
11	100-250	585	Z2/Z4	50314	53091.15	-0.2

The analysis of the Table 5 and 6 suggests that generally both bulk conductivity and magnetic intensity tend to decrease when passing from unaltered to altered sandstone. The decrease in bulk conductivity ranges from 8 to 36 % while that of magnetic field varies from 0.2 to 3.2%. On the other hand, there are a lot of fluctuations on geophysical profile of the zone 2 alone. The fluctuations are due to the presence of various sources of interference. In most cases the rate of fluctuation can easily exceed 3%. This implies that it might be a little bit difficult to differentiate between the variation of magnetic intensity due to source of interference and those due to the contact between zone 2 and zone 4 especially if the presence of the zone 2 is not known in advance.

Table 6: Variation of Bulk Conductivity (Q) in 4 intervals where there was higher probability to cross the boundary between the altered sandstone (Zone 2) and the unaltered sandstone (Zone 4).

Line #	Interval (m)	Location (m)	Zone Boundary Z_2/Z_4	Background Conductivity (mSm)	Max Conductivity (mSm)	Increment %
0	150-250	215	Z2/Z4	43	95	-36
6	650-750		Z2/Z4			
7	0-50	35	Z2/Z4	28	33	-8.6
11	100-250	175	Z2/Z4	22	35	-29.04

3. Delineation of pyrite zone

Previous studies have already reported the occurrence of pyrite in several locations of the study area. Pyrite horizons are usually found in the bleached sandstone of the Rush Springs Formation where they occur as cementing nodule or as disseminated cubes in calcite area (Fegurson, 1977; Al-Shaieb 1988). Unlike ridges of calcite, pyrite crystals are found in small veinlets where they are associated with marcasite nodules (minor constituents) and native sulfur (Lilburn, 1981; Al-Shaieb, 1988).

On the other hand, a detailed study on well Logs in the study area revealed the presence of pyrite horizons in the Davis, Cothlin and in the Pekaune No 1 wells (Reeves, 1921). Pekaune No 1 well is located about 150 m west from station 590 m on the line 9. In this well, pyrite horizons have been intercepted at the depth interval of 194 – 233 m, 555- 560 m and 563-567 m. Pyrite horizons in Pekaune No 1 well occurs either in shale or in carbonate rock "limerock".

Though the present geophysical investigation was imaging the subsurface down to 15m (VD: EM 34), the anomalous reading of the magnetic intensity recorded in the vicinity of the station 590 m on the line 9 could only be explained by the presence of E-W faults inferred from the aeromagnetic data and which was confirmed in the previous study.

It is also important to note that, most of the time, during the present survey, higher bulk conductivities were recorded in the vicinity of stations characterized by high magnetic intensity. This situation can be explained either by the simultaneous occurrence of both magnetite and pyrite on the same fractures (Reynolds et al., 1990), or by the presence of pyrrotite alone which have already been reported in the study area (Lilburn, 1981; Al-Shaieb, 1988). In any case, the

complexity of bulk conductivity in the anomalous areas suggests that there were more than one mineral precipitates.

The conditions of precipitation pyrite have been a subject of several discussions (Meyer et al., 1967; Rose et al., 1979; Evans, 1987). In Australia, the occurrence of authigenic pyrite in the seepage areas, in the middle Jurassic Laminaria and Plover sandstone Formations, has been interpreted as resulting from the reaction between iron oxide and hydrogen sulfide. The hydrogen sulfide originated from the reduction of sulfate water in the presence migrating hydrocarbon (Beydoun, 2014). The presence of migrated hydrocarbon which played an important role in the metabolism of sulfate reducing microorganisms is emphasized in this model. On the other hand, the abiotic precipitation of pyrite due to diffusion of H_2S through a porous media of hydroxide iron is possible under anaerobic conditions (Schlesinger et al., 2013). This second model has been recommended for the HIDA in the Cement oil field based on isotopes analysis δS^{34} (Al-Shaieb, 1988; Lilburn, 1981, Puckette et al., 2011). The discoloration of Permian beds implies the presence of acidic fluids that reduced iron oxide (hematite) to precipitate pyrite (Yaron et al., 2012).

Indeed a close analysis of the occurrence of pyrite in the Cement oil field reveals that pyrite occurs either as disseminated in the sandstone or as nodule in the calcite extended zone. The dissemination of pyrite in the bleached sandstone zone can be interpreted as due to the diffusion of the hydrogen sulfide through iron hydroxide, while the occurrence of pyrite nodule in the carbonate cemented sandstone zone is mostly due to the chemical reactions between at least two types of waters. The reduction between water rich in sulfate ions by the waters rich in carbonate

ions that most likely took place within the fractures (or fault zones) were catalyzed by appropriate microbial activities and enhanced the growth of calcite the walls of discontinuities.

Indeed experiment in the lab between 25-45 degrees Celsius shows that when polysulfides react with Fe^{2+}, FeS which is the first product to form (equation 3-6) (Luther, 1991; Rickard et al., 1975, Rickard et al., 1997) can react abiotically with H_2S to precipitate pyrite (Schlesinger et al., 2013).

$$FeS + H_2S <==> FeS_2 + 2H^+ + 2e^- \quad (3)$$

$$(H_2S <==> H^+ + HS^- \quad Ks = 8.9 \times 10^{-8}) \quad (4)$$

$$2\ Fe(OH)_3 + 2\ H_2S + H_2 <==> 2FeS + 6H_2O \quad (5)$$

$$(HS^- <==> H^+ + S^{2--} \quad Ks = 1.2 \times 10^{-13}) \quad (6)$$

4. Delineation of calcite zone

The fact that carbonate cemented sandstone is more competent than the rest of the surrounding friable Rush Springs Sandstone, explains why they occur as ridges throughout the Cement oil field. Indeed many studies of long term hydrocarbon seeps confirm the development of authigenic calcite (carbonate) along faults walls to form ridges or mounds (Stakes et al., 1999). The development can include continuous pavements, shallow sediments, cemented conduits, carbonate veins of ankerite or calcite like in the gulf of Mexico (Simoneit et al., 1990; Stakes et al, 1999). The "occurrence of carbonate cemented sandstone can be easily traced down in the deeper depth, even below the sediment water "(Naehr et al., 2007 and 2009).

Can the presence of carbonate cemented zones be used in the hydrocarbon exploration? As mentioned earlier, given that the precipitation of carbonate minerals along the fault walls can be enhanced by ascending light hydrocarbon from the seeps, the method of exploration of shallow hydrocarbon based on the identification of carbonate ridges (Al-Shaieb, 1988) can find its justification. Indeed the sharp contact between carbonate cemented sandstone and the country rock have helped and can still help to delineate carbonate cemented sandstone (zone 1) which is related to the presence of hydrocarbon. Though some carbonate ridges have already been mapped (Allen, 1980) in the study area, the present geophysical investigation have managed to identify many more outcrops.

As far as the conditions of precipitation of carbonate minerals are concerned, there are several paths that can lead to the precipitation of carbonate minerals (Castanier et al., 1999). The abiotic path depends mainly on temperature, pressure agitation, sediment masking and clogging, light (photic zone) and carbonate Compensation Depth (CCD) (McKinnon, 2011). Indeed when inorganic carbon dioxide is dissolved in water (DIC), Dissolved inorganic carbon is partitioned between bicarbonate, carbonate and the proportion of each depends on the PH (Schlesinger et al., 2013). Carbonate ions can combine with calcium to form calcite, ferroan calcite. Manganese rich calcite carbonate ions can combined with other metals such as magnesium to form dolomite and ankerite (Al-Shaieb, 1988).

Experiment in the Lab confirms that, in addition to the parameters that induces abiotic precipitation of calcite, the presence of sulfate of calcium (gypsum) and that of assimilable organic matter (Kellerman, 1914; Smith, 1940; Lalou, 1957) are very important for efficient

precipitation. Gypsum plays an important role in reducing the solubility of carbonate minerals such as calcite due to the common ions effect, hence inducing more calcite precipitation.

In the Cement oil field, the analysis of δC13 isotopes of carbonate sandstone based on 144 mineral samples suggests 3 major sources of carbon. The first source (organic) is characterized by the value of δC13 around -32 ‰ vs PDB. The δC13 value of the second source varies between--8+/-13 ‰ and the third source is interpreted to be hybrid between the two (Puckette et al., 2011). To some extent this conclusion supports the Drake et al. (2014) model that describes two sources fluids that contribute to the precipitation of calcite in the fractured granite. The descending sulfate poor fluids that contain methane percolated through fractures where they encountered sulfate rich water but poor in bicarbonate ions.

5. Model

As mentioned earlier, several models have already been proposed for the HIDA in the Cement oil field. In addition to the results observed in the field, the present model (Figure 30) takes into consideration the geophysical data collected throughout the present survey. The Model can be subdivided into 7 phases:

(1) The exhumation of light hydrocarbons (Methane, Ethane up to butane) from the seeps was progressive and was accompanied by hydrogen sulfide.

(2) Local ground water which was enriched in sulfate ions due to the presence of gypsum, percolated through different network of fractures (faults and other discontinuities) and enhanced chemical reactions between light hydrocarbons and ground waters. These reactions (equation 7) that took place under anaerobic conditions, were catalyzed by

microorganism activities and resulted in the precipitation of carbonate minerals and production of more hydrogen sulfide.

$CH_4 + SO_4^{2-} <==.>. HCO_3^- + HS^- + H_2O$ (7)

(3) Once produced, the hydrogen sulfide diffused through iron hydroxides present in the Permian sequences (Donovan, 1972; Ferguson, 1977) and reacted abiotically to precipitate "cemented pyrite" (equation 8).

$2\ Fe(OH)_3 + 2\ H_2S + H_2 <== > 2FeS + 6H_2O$ (8)

(4) With the help of microorganisms, dissolved hydrogen sulfide reacted with sulfate water and precipitated crystal of pyrite that has been observed in the carbonate cemented zone (along the plane of discontinuity, veins and veinlets).

(5) hydrogen sulfide that could not react with surface water, escaped through the seeps, network of fractures and later on reacted under aerobic conditions to form sulfate minerals.

(6) On the other hand, while ascending progressively towards the earth surface, part of light hydrocarbon (Methane) dissolved in water ended up by being oxidized under aerobic conditions (with help of microbial activities) and produced more carbon dioxides that oversaturated surface water in CO_3^{2-} (equation 9) and HCO_3^-, consequently enhanced more precipitation of carbonate minerals.

$CH_4 + 2O_2 == > CO_2 + 2H_2O$ (9)

Part of methane that escaped up to the earth surface could not be oxidized under aerobic conditions and evaporated straight into atmosphere.

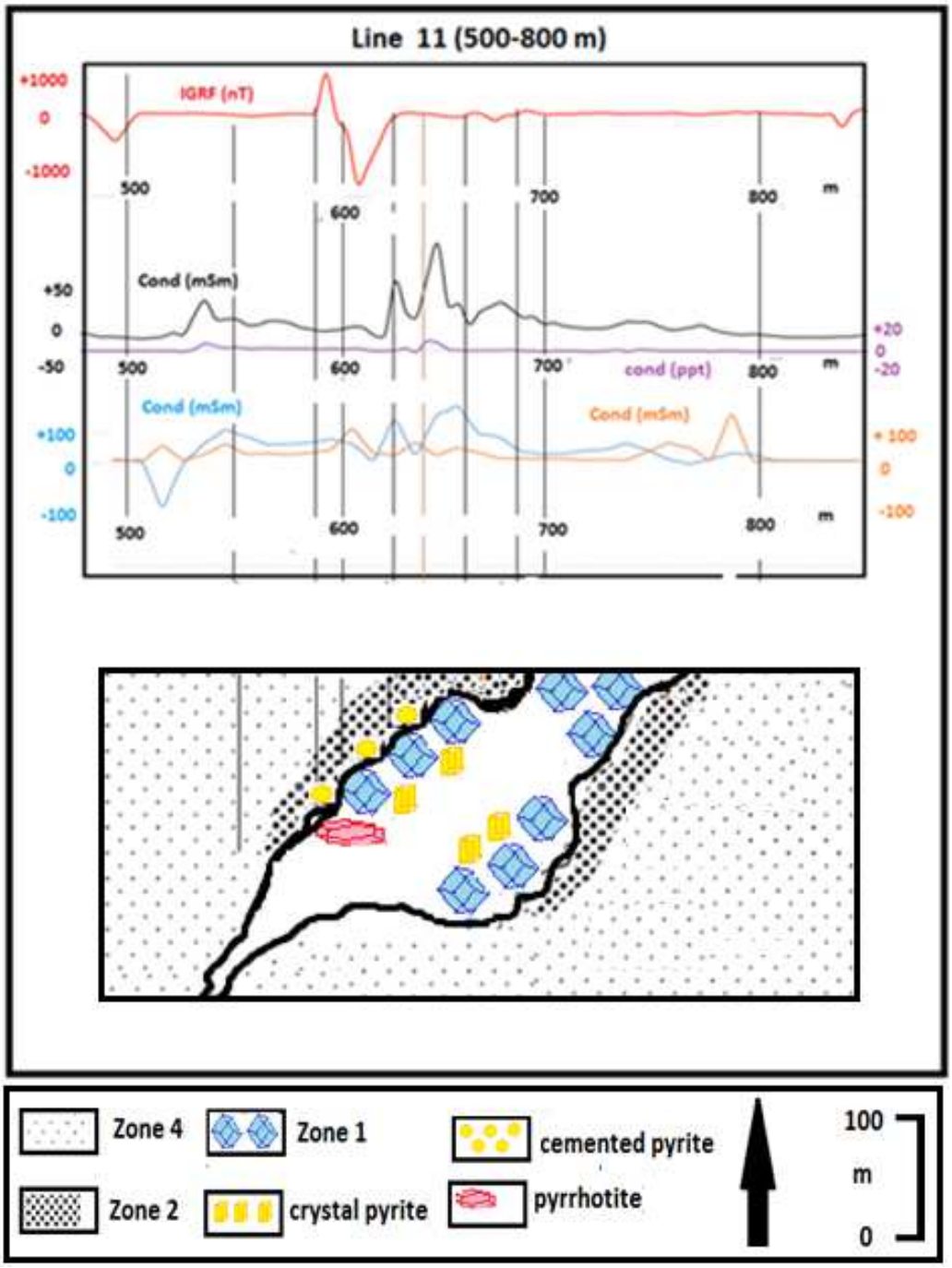

Figure 30: Model based on the present electromagnetic and magnetic survey with EM 31, EM34 and G858 cesium magnetometer respectively, on line 11. Though this model is a cursory interpretation of the subsurface alteration in the interval between 500-800 m, it illustrates the spatial relationship between the 4 zones.

CHAPTER V

CONCLUSION

The electromagnetic and magnetic investigations undertaken in the Cement oil field have revealed that at the boundary between the unaltered (zone 4) and altered Rush Springs Sandstone (zone 2) both the bulk conductivity and the total magnetic intensity tend to decrease. The decrease in the magnetic intensity ranges from 0.2% to 3.2% and that of the bulk conductivity from 8 to 30%. These variations would be difficult to perceive. The decrease in both bulk conductivity and magnetic intensity result from the difference in the physical properties between sandstone and carbonate cemented sandstone rather than in the presence of hydrocarbon.

The geophysical survey at the boundary between sulfide (zone 3) and carbonate cemented sandstone (zone 1) shows that the signature of both bulk conductivity and magnetic intensity are somehow mixed in the vicinity of fault zones. The mixing in the signature is interpreted as due to the accumulation of different types of carbonate minerals. To some extent the boundary between sulfide (zone 3) and altered sandstone (zone 2) is difficult to differentiate from sulfide (zone 3) and carbonate cemented sandstone (zone 1). In any case the contrast between the background and the maximum values ranges from 0.53 to 10% for the magnetic intensity and up to 600% for the bulk conductivity. This suggests that the detection of the boundary of sulfide zone would be more efficient with EM31 than with G858 Cesium magnetometer.

The precipitation of pyrite in the HIDA of the Cement oil field is here confirmed to be the result of the reaction of iron oxides with hydrogen sulfide that came from the reduction of sulfate water in the presence of entrapped oil. It could also due to the diffusion of H_2S through a porous media of hydroxide iron in sandstone. The reduction of iron oxide under anaerobic condition that result in the precipitation of pyrite was accompanied with the change in color that characterizes the flank of calcite ridges. The bleaching of red bed sandstone could have also resulted from the secondary deposition of calcite.

The presence of several carbonate cemented sandstone ridges suggest a continuous process of accumulation of carbonate minerals for a longer period. Carbonate minerals were accumulated as a result of chemical reaction between mixed waters from at least three sources. Aerobic and anaerobic oxidations of methane contributed tremendously in the carbonate ions saturation. However, the presence of gypsum played an important role in reducing the solubility of carbonate minerals in solution due to the common ions effect and induced more carbonate minerals precipitation. Other factors such as microbial activities, presence of light, hydrogen sulfide, sulfate waters from various sources increased considerably the precipitation of a number of carbonate minerals that comprise mainly several varieties of calcite, dolomite and ankerite.

Hence, geophysical techniques have efficiently detected the boundary between the sulfide zone and carbonate cemented sandstone in the HIDA of the Cement oil field. It can also locate long term hydrocarbon seeps based on the detection of calcite ridges, or based on the change in color between unaltered and altered sandstone.

REFERENCES

Allen, R.F., 1980, Uranium potential of the Cement District, southwestern Oklahoma [Unpublished, M.S. Thesis]: Stillwater, Oklahoma State University, 84 p.

Al-Shaieb, Z., 1988, Hydrocarbon-induced diagenetic aureole at Cement-Chickasha anticline: Oklahoma, Geological Society America, Centennial Field Guide, South-Central Section, v.4, p.104-108.

Atekwana, E.A., Sauck, W.A., Werkema, D.D., 2000, Investigations of geoelectrical signatures at a hydrocarbon contaminated site: Journal of Applied. Geophysics, v. 44, Issues 2-3, p.167-180.

Atekwana. E.A., Atekwana, E.A., Werkema, D.D., Allen, J.P., Smart, L.A., Duris, W.J., Cassidy, D.P., Sauck, W.A., Rossbach, S., 2004 Evidence, for microbial enhanced electrical conductivity in hydrocarbon-contaminated sediments: Geophysical Research Letters, v.31, l23501,p.1-4

Atekwana, E. A**.,**. Slater, L. D, 2009, Biogeophysics: A new frontier in earth science research: Review of Geophysics, 47

Atekwana, E.A., Atekwana, E.A., 2010, Geophysical signatures of microbial activity at hydrocarbon contaminated Sites: A Review: Survey Geophysics, v.31, p.247-283.

Atekwana, E.A., Mewafy, F.M., Aal, G.A., Werkema D.D.Jr., Revil, A., Slater, L.D., 2014, High-resolution magnetic susceptibility measurements for investigating magnetic mineral formation during microbial mediated iron reduction: Journal of Geophysical Research, Biogeosciences, v. 119, p.80-94.

Barriol, Y., Bartman, B., Corbiell, R., Eriksen, O.K., Laidlaw, J., Manin, Y., Morrison, K., Sayers, M.C., Romero, M.T.T., Volokitin, Y., 2006, The pressures of drilling and production: https://www.slb.com (Accessed February 2015).

Beydoun, Z., 2014, Late Authigenic Pyrite - An Indicator of oil migration and entrapment in the Bonaparte Basin, Timor Sea, Australia: Association for American Petroleum Geologist, International Conference and Exhibition Istanbul: www.searchanddiscovery.com (Accessed August 2015).

Brant, A.A., Dolan, W.H., and Elliot, C.L., 1966, Coplanar and coaxial EM tests in Bathurst area: in Mining Geophysics*,* Case Histories: Society of Exploration Geophysicists, p.130-141.

Breiner, S., 1973, Applications Manual for Portable magnetometer, 58p: ftp://geom.geometrics.com/pub/mag/literature/ampm-opt.pdf (Accessed June 2014)

Bruce, H.H., 1960, Stratigraphy of Cement Pool and Adjacent Area, Caddo and Grady Counties, Oklahoma: Bulletin of the American Association of Petroleum Geologists, vol. 44, No.2, p.210-226.

Burger, H.R., Sheehan, A.F., Jones, C.H., 2006, Introduction to Applied Geophysics: NewYork-London, W.W. Norton and Company, 554 p.

Cannon, R. A., Rice, G.K., Belt, J. Q. Jr., 2001, How Integrated Modeling Assisted with Navigator Find, Midland Basin Eastern Shelf": Oil and Gas Journal, in http://www.geofrontiers.com/Navigator

Castanier, S., Levrel, G.M., Perthuisot, J.P, 1999, Ca-carbonates precipitation and limestone genesis – the microbiologist point of view: Sedimentary Geology, v.126, p.9-23.

Clarke, R.H., Cleverly, R.W., 1991, Petroleum seepage and post accumulation migration: in England WA., Fleet AJ, eds, Petroleum migration: Geological Society special publication, Geological Society of London, v.59, p.265-271.

Clayton, C.J., 1991, Carbon isotope fractionation during natural gas generation from kerogen: Marine and Petroleum Geology, v.8, p.232-240.

Clayton, C.J., Lines, M.D., Hay, S.J., 1991, Leakage and seepage, an explorer guide: BP internal report, now available from Robertson Research International, 65 p. in Barry D., 2001, Hazardous Gases Underground: Applications to Tunnel Engineering New York, https://books.google.com/books (Accessed May 2015).

Clayton, J.L., Konca, I., 1991, Application of organic geochemistry to petroleum exploration in Bekes Basin: Hungary: in Association American Petroleum Geologist Bulletin, v. 75:3, 554p.

Donovan, T.J., 1972, Surface Mineralogical and Chemical evidence for Buried Hydrocarbons, Cement Field Oklahoma [Ph.D. thesis]: Los Angeles, University of California, 117 p.

Desai, A., Vyas, P., 2006, Applied Microbiology, Petroleum and Hydrocarbon Microbiology: University of Baroda, 22 p., in nsdl.niscair.res.in (Accessed October 2015).

Drake, H., Åstro, M.E., Heim, C., Broman, C., Åstro, J., Whitehouse, M., Ivarsson, M., Siljestro, S., vall, P.S., 2015, Extreme ^{13}C depletion of carbonates formed during, oxidation of biogenic methane in fractured granite: Macmillan, in Nature communications: http://www.nature.com (Accessed July 2015).

Duran, P.B., 2014, The Effects of Cultural and Natural Interference on Electromagnetic Conductivity Data: info.ngwa.org/gwol/pdf/082383241.pdf (Accessed June 2015).

Evans, A.M., 1987, Textures and structures of ore and gangue minerals. Fluid inclusions. Wall rock alteration, in Evans, A.M., ed 3., Ore Geology Industrial Minerals An introduction: London, Blackwell Sciences, 390 p.

Fegurson, J.D., 1977, The subsurface alteration and mineralization of Permian red beds overlying several oil fields in southern Oklahoma [Unpublished, MS. Thesis]: Stillwater, Oklahoma State University, 95 p.

Fu, B., Zheng, G., Ninomiya, Y., Wang, C., Sun, G., 2007, Mapping hydrocarbon-induced mineralogical alteration in the northern Tian Shan using ASTER multispectral data: Blackwell, Terra Nova, vol. 19. No4, p. 225-231.

Geomatrix, 2015, Land Geophysical Equipment: Electromagnetic: Geonics EM31-MK2: http://www.geomatrix.co.uk/products/land-geophysical-equipment/electromagnetic/em31-mk2/ (Accessed January 2015).

Geometrics,2001, Magmapper, Operation Manual: www.geo.mtu.edu/.../858Manual_D *(Accessed, January 2015).*

Gilbert, M.C., 1983, Timing and chemistry of igneous events associated with the southern Oklahoma aulacogen: Elsevier Science, Tectonophysics, v. 94, p. 439–455.

Gilbert, M.C., 1987, Petrographic and structural evidence from the igneous suite in the Wichita Mountains bearing on the Cambrian tectonic style of the Southern Oklahoma aulacogen: Geological Society of America Abstracts with Programs, v. 19, No. 3, p. 152.

Gluyas, J; Swarbrick, R., 2004, Petroleum Geoscience: Blackwell Publishing. http://www.academia.edu/317834 (Accessed March 2015).

Gorton, G. A ,1975 "Big-Ass Boy" in the Oil Fields: My Adventures, 1918–28 (N.p.: N.p., 1975). in Cement: Encyclopedia of Oklahoma History and Culture: http://www.okhistory.org/publications (Accessed January 2015).

Hubert C., Judd, A., 2010, Using Microorganisms as Prospecting Agents in Oil and Gas Exploration, *in* Timmis , K.N., 2010, Handbook of hydrocarbon and Lipid Microbiology: Germany, Springer-Verlag Berlin Heidelberg, v1-5, 4699 p.

Ihsan, S.R., Nordiana, M.M., Saad, R., Saidin, M., Maslinda, U., Hisham, H., Sulaiman, N., 2015, Investigation of Ancient River at Lembah Bujang, Kedah, Malaysia: Electronic Journal of Geotechnical Engineering, v.20, p.4385-4392.

*Keller, G.R., Stephenson, R.A., 2007, The southern Oklahoma and Dniepr-Donets aulacogens: A comparative analysis: in Hatcher, R.D., Jr., Carlson, M.P., McBride, J.H., and Martinez Catalán, J.R., eds., 4-D Framework of continental crust: Geological Society of America Memoir 200, p.127–143.

Kellerman, K.F., Smith, N.R., 1914, Bacterial precipitation of calcium carbonate: Washington Academy, Science Journal, V.4, p. 400-402.

Khan, S.D., Jacobson, S., 2008, Remote sensing and geochemistry for detecting hydrocarbon microseepages: Geological Society of America Bulletin, v.120, No1-2, p.96-105.

Lalou, C., 1957, Studies on bacterial precipitation of carbonates in sea water: Journal of Sedimentary Petrology, v.27, No 2, p.190-195.

Lilburn, R.A., and Al-Shaieb, Z., 1983, Geochemistry and isotopic composition of hydrocarbon-induced diagenetic aureole (HIDA), Cement, Oklahoma: Shale Shaker, pt. H. v.34. No5. P.57-67.

Lilburn, R.A., 1981, Mineralogical, geochemical, and isotopic evidence of diagenetic alteration, attributable to Hydrocarbon migration, Cement –Chikasha field [Unpublished, M.S. Thesis]: Stillwater, Oklahoma State University, 88p.

Luther G.W., 1991, Pyrite synthesis via polysulfide compounds: Geochimica Cosmochimica Acta, v.55, p.2839-2849.

Marescot, L., 2015*, Basic theory: Induction Electromagnetic Surveying: www.tomoquest.com/attachments/ (Accessed May 2015).

Mewafy, F. M., Atekwana, E. A, Werkema D.D. Jr., Slater L. D., Ntarlagiannis, D., Revil, A., Skold, M., Delin, G. N, 2011, Magnetic susceptibility as a proxy for investigating microbially mediated iron reduction: Geophysical Research Letters, v.38, p.1-5.

Meyer, C., Hemley, J.J., 1967, Wall rock alteration: in New York, Geochemistry of hydrothermal ore deposits, Barnes H.L., ed., Holt, Rinehart and Winstone, p. 166-232. In The mineralogical characteristics and the zoning of the hydrothermal types alteration from Nistru Ore deposit, Baia Mare Metallogenetic Distric. Studia Universitatis Babes-Bolyai, Geologia, v.18, p.101-112.

McKinnon, M., 2013, Carbonate Precipitation: http://www.geomika.com (Accessed June 2015).

Naehr, T.H., Eichhubl, P., Orphan, V.J., Hovland, M., Paull, K.C., Ussler III, W., Lorenson, T.D., Greene, G.H., 2007, Authigenic carbonate formation at hydrocarbon seeps in continental margin sediments: A comparative study: Science Direct, Deep sea Research, v.54, p.1268-1291.

Naehr, T.H., Birgel, D., Bohrmann, G., MacDonald I.R., Kasten, S., 2009, Biogeochemical controls on authigenic carbonate formation at the Chapopote "asphalt volcano", Bay of Campeche: Elsevier , chemical geology , v.266, p. 390-402.

Olmstead, R.W., 1975, Geochemical studies of uranium in south-central Oklahoma [unpublished, M.S. Thesis]: Stillwater, Oklahoma State University, 116 p.

Palacky, G.V., 1987, Geophysics foundations: Physical properties: Electrical resistivity of geologic materials: http://www.eos.ubc.ca (Accessed May 2015).

Parasnis, D.S., 1956, The electrical resistivity of some sulfides and oxide minerals and their ores: Geophysics Press, in Pearce, C. I., 2006, Electrical and Magnetic Properties of Sulfides: Reviews in Mineralogy and Geochemistry, v. 61, No. 1, p. 127-180.

Pearce, C. I., 2006, Electrical and Magnetic Properties of Sulfides: Reviews in Mineralogy and Geochemistry, v. 61, No. 1, p. 127-180.

Pearson, O.N., Higley, D.K., Miller, J.J., 2014, Tectonic and Structural Evolution of the Anadarko Basin and Structural Interpretation and Modeling of a Composite Regional 2D Seismic Line: Chapter 11 of 13, Petroleum Systems and Assessment of Undiscovered Oil and Gas in the Anadarko Basin Province, Colorado, Kansas,

Perez, A., D'Onofrio, L., Bosch, M., Zapata, E., 2011, Association between magnetic susceptibilities and hydrocarbon deposits in the Barinas-Apure Basin, Venezuela: Geophysics, v.76, No 6, L35-L41.

Perry, J.J., Williams, S., 1968, Oxidation of hydrocarbons by microorganisms isolated from soil. Canadian Journal of Microbiology, v.14, p.403–407.

Petrovic, A., Khan, S. D., Chafetz, H. S., 2008, Remote detection and geochemical studies for finding hydrocarbon-induced alterations in Lisbon Valley, Utah: Marine and Petroleum Geology, v. 25, No. 8, p. 696-705.

Price, L.C., 1986, A critical overview of and proposed working model for hydrocarbon microseepage Open-File Report 85-271: http://pubs.er.usgs.gov/publication/ofr85271 (Accessed October 2015).

Puckette, J., Dressler, D., Bagley, E., 2011, Guidebook to the Hydrocarbon leakage induced diagenetic alteration over Cement oil field, OKlahoma: *in* 2011 mid Continent section meeting American Association of Petroleum Geologist, Oklahoma State University, 18 p.

Rackley, N., 2002, comp., Cement, Oklahoma, 1902–2002: Footprints of Its First Hundred Years in (Rich Hill, Mo.: Bell Books, 2002). in Cement: Encyclopedia of Oklahoma History and Culture: http://www.okhistory.org/publications (Accessed January 2015).

Rasheed, M. A., Lakshmi, M., Srinu, D., Dayal, A.M., 2011, Bacteria as indicators for finding oil and gas reservoirs: A case study of the Bikaner-Nagaur Basin, Rajasthan, India: Petroleum Science, v. 8, No. 3, p. 264-268.

Rasheed, M.A., Patil, D.J., Dayal, A.M., 2013, Microbial Techniques for Hydrocarbon Exploration: http://www.intechopen.com/books/hydrocarbon, (Accessed July 2015).

Reeves, F., 1921, Geology of the Cement oil field, Caddo County, Oklahoma: Pubs.usgs.gov/bul/0726b/report.pdf (Accessed January 2015).

Reynolds, R.I., Fishman, N.S., Wanty, B.R., Goldhaber, B.M., 1990, Iron sulfide minerals at Cement oil field, Oklahoma: Implications for magnetic detection of oil fields: Geological Society of America Bulletin, V.102, p.368-380.

Rickard, D.T., 1975, Kinetics and mechanisms of pyrite formation at low temperatures: in Rickard, D., Luther, G.W., 1997, Kinetics of pyrite formation by the H_2S oxidation of iron (ii) monosulfide in aqueous solutions between 25and 125^o C: The mechanism: Elsevier Science, Geochimica et Cosmochimica Acta, v. 61, No.1, p. 135-147.

Rickard, D., Luther, G.W., 1997, Kinetics of pyrite formation by the H_2S oxidation of iron (ii) monosulfide in aqueous solutions between 25and 125^o C: The rate equation: Elsevier Science, Geochimica et Cosmochimica Acta, v. 61, No.1, p. 115-134.

Rickard, D., Luther, G.W., 1997, Kinetics of pyrite formation by the H_2S oxidation of iron (ii) monosulfide in aqueous solutions between 25and 125^o C: The mechanism: Elsevier Science, Geochimica et Cosmochimica Acta, v. 61, No.1, p. 135-147.

Rijal, M. L., Appel, E., Petrovsky, E., and Blaha, U., 2010, Change of magnetic properties due to fluctuations of hydrocarbon contaminated groundwater in unconsolidated sediments: Environment Pollution, v. 158, No. 5, p. 1756-1762.

Rose, A.W., Burt, D.M., 1979, Hydrothermal alteration In Barnes H.I. ed., geochemistry of hydrothermal Ores deposits: Hott Rinchart and Winston, p.166-235.

Saunders, D.F., Burson, K.R, Thompson, C.K., 1999, Model for Hydrocarbon Microseepage and Related Near-Surface Alterations: Association of American Petroleum Geologist Bulletin, v 83, No. 1, p.170–185.

Sundberg, K.R., 1994, Surface geochemistry applications in oil and gas exploration: Oil Gas J 92(23): 47–56, *in* Hubert C., Judd, A., 2010, Using Microorganisms as Prospecting Agents in Oil and Gas Exploration: in Timmis, K.N., 2010, Handbook of hydrocarbon and Lipid Microbiology: Germany, Springer-Verlag Berlin Heidelberg, v.1-5, 4699 p.

Schlesinger, W.H., Emily, S.B, 2013, Biogeochemistry, An analysis of global change: New York, Academic press, 672 p.

Schumacher, D. H., 1996, Hydrocarbon-Induced Alteration of Soils and Sediments, *in* Schumacher Abrams, M.A., eds, Hydrocarbon migration and its–surface expression: Association of American Petroleum Geologists, Memoir 66, p.71-89.

Schumacher, D. H., Tucker, J., Rountree, B., 2011, Applying high-resolution surface geochemistry to assess reservoir compartmentalization and monitor hydrocarbon drainage, *in* Kruizenga, R.J., Downey, M.W. eds., Applications of Emerging Technologies: in Rasheed, M.A., Patil, D.J., Dayal, A.M., Microbial Techniques for Hydrocarbon Exploration.

Simoneit, B.R.T., Lonsdale, P.F., Edmond, J.M., Shanks, I.W.C., 1990, Deep-water hydrocarbon seeps in Guaymas Basin, Gulf of California: Applied Geochemistry, v.5, p.41–49.

Smith, C.L., 1940, The great Bank of Bahamas II. Precipitation of calcium carbonates: journal, Mar. res, V.3, 171 p. in Lalou, C., 1957, Studies on bacterial precipitation of carbonates in sea water: Journal of sedimentary petrology, v.27,. No 2, p.190-195.

Stakes, D.S., Holloway, G.L., Tucker, P., Dawe, T.C., Burton, D., McFarlane, J.A.R., Etchemendy, S., 1997, Diamond Rotary Coring from an ROV or Submersible for Hardrock Sample Recovery and Instrument Deployment: The MBARI Multiple- Barrel Rock Coring System: Marine Technology, Society Journal, v.31, No, p.11-20.

Stakes, D.S., Orange, D., Paduan, B.J., Salamy, K.A., Maher, N., 1999, Cold-seeps and authigenic carbonate formation in Monterey Bay, California: Marine Science, v.159, p.93-109.

Stone, V.C.A, Farhead, D.F., 2004, Micromagnetic seep detection in the Sudan: http://tle.geoscienceworld.org/content/23/8/734.extract (Accessed August 2013)

Telford, W.M., Geldart, L.P., Sheriff, R.E., Keys, D.A., 1976, Applied Geophysics, Cambridge University Press: New York, 860 p.

Thomas, W.A., 1977, Evolution of Appalachian-Ouachita salients and recesses from reentrants and promotories in the continental margin: American Journal of Sciences, v. 277, p.1233-1278.

Thomas, W.A., 1975, Appalachian Ouachita structure and plate tectonics: Abstracts, Geological America Abstracts with programs, v.7, p.543-544.

Timothy, T., 2015, Overhead clearances for conductors and cables for 600 Volts or Less: http://electrical.about.com (Accessed October 2015).

TurnBull, G., 2013, Maxwell's equations scanning our past, history Center: Proceedings of the Institute Electrical and Electronical Engineers, v.101, No7, p.1801-1805.

Pearce, C.I., Vaughan, D.J., Patrick, R.A.D., 2006, Electrical and Magnetic Properties of Sulfides: Reviews in Mineralogy and Geochemistry, v.61, p.127-180.

Williams, A., Lawrence, G., 2002, The Role of Satellite Seep Detection in Exploring the South Atlantic's Ultradeep Water: in Surface exploration case histories: Applications of geochemistry, magnetics, and remote sensing. D. Shumacher and L. A. Leschak, eds., Association of American Petroleum Geologists, Society of Exploration Geophysicists, Geophysical References Series, No. 11, p. 327-344.

Wilson, S., 1976, Oklahoma Treasures and Treasure Tales (Norman: University of Oklahoma Press, 1976) in Cement: Encyclopedia of Oklahoma History and Culture: http://www.okhistory.org/publications (Accessed January 2015)

Vestal, J.R., Perry, J.J., 1971, Effect of substrate on the lipids of the hydrocarbon utilizing Mycobacterium vaccae: Canadian Journal of Microbiology, v.17: 445-449.

Yaron, B., Dror, I., Berkowitz, B., 2012, Soil-Subsurface Change, Chemical Pollutant Impacts: New York, Springer Heidelberg Dorrecht, London, 366 p.

APPENDICES

Annex- 1

Def stn	Easting	Northing	Line#	MAG(nT)	IGRF(nT)	Q(mS/m)	I(mS/m)	VD(mS/m)	HD(mS/m)
0	578500	3864700	0	49851.585	-513.32636	64	20	67	41
1	578500	3864705	0	50131.497	-233.42764	60	20	55.5	41
2	578500	3864710	0	50112.862	-252.07593	40	4	44	41
3	578500	3864715	0	50125.096	-239.85522	46	1	42.5	42
4	578500	3864720	0	50196.454	-168.51051	43	-1	41	43
5	578500	3864725	0	50220.942	-144.0358	45	0.2	38	43
6	578500	3864730	0	50250.616	-114.37509	43	0.7	35	43
7	578500	3864735	0	50259.621	-105.38338	43	-0.1	38.5	44
8	578500	3864740	0	50261.703	-103.31466	42	-1	42	45
9	578500	3864745	0	50254.814	-110.21695	42	-1	38.5	45
10	578500	3864750	0	50245.923	-119.12124	44	-1	35	45
11	578500	3864755	0	50207.87	-157.18753	47	-1	56	45
12	578500	3864760	0	50166.56	-198.51081	51	-1	77	45
13	578500	3864765	0	49966.663	-398.42111	61	-0.3	-1	43
14	578500	3864770	0	45800.135	-4564.9624	72	0.1	-79	41
15	578500	3864775	0	43732.004	-6633.1067	80	1	-16.5	43.5
16	578500	3864780	0	48290.132	-2074.992	70	0.9	46	46
17	578500	3864785	0	50562.857	197.71974	60	0.1	50	45.5
18	578500	3864790	0	50202.708	-162.44255	47	-1	54	45
19	578500	3864795	0	50163.183	-201.98083	41	-1	65.5	45.5
20	578500	3864800	0	50159.333	-205.84412	37	-1	77	46
21	578500	3864805	0	50200.268	-164.92241	40	-0.9	21	44
22	578500	3864810	0	50228.356	-136.8477	47	0.1	-35	42
23	578500	3864815	0	50199.752	-165.46498	18	-3	6.5	48
24	578500	3864820	0	50182.673	-182.55727	52	0.4	48	54
25	578500	3864825	0	50122.528	-242.71556	46	-0.5	46	54.5

.

Def stn	easting	Northing	Line#	MAG(nT)	IGRF(nT)	Q(mS/m)	I(ppt)	VD(mS/m)	HD(mS/m)
26	578500	3864830	0	50192.005	-173.25185	47	-0.5	44	55
27	578500	3864835	0	50226.043	-139.22713	49	-0.7	47	53
28	578500	3864840	0	50216.959	-148.32443	49	0.5	50	51
29	578500	3864845	0	50237.989	-127.30771	45	-0.7	50.5	50
30	578500	3864850	0	50266.999	-98.310997	42	-0.6	51	49
31	578500	3864855	0	50262.361	-102.96228	42	-0.3	49	48
32	578500	3864860	0	50256.2	-109.13658	51	0.6	47	47
33	578500	3864865	0	50235.114	-130.23586	61	2	56.5	46.5
34	578500	3864870	0	50199.14	-166.22315	28	-3	66	46
35	578500	3864875	0	50117.893	-247.48344	48	1	61	42.5
37	578500	3864885	0	48754.487	-1610.916	39	-0.7	51	43.5
38	578500	3864890	0	50202.304	-163.1123	38	-0.8	46	48
39	578500	3864895	0	50983.096	617.66641	39	-1	49	50
40	578500	3864900	0	50312.893	-52.549873	41	-0.9	52	52
41	578500	3864905	0	50323.836	-41.620159	46	-0.1	60.5	56
42	578500	3864910	0	50204.553	-160.91645	55	1	69	60
43	578500	3864915	0	50316.311	-49.171736	95	10	-16.5	54
44	578500	3864920	0	50331.717	-33.779022	-11	-13	-102	48
51	578500	3864955	0	42519.424	-7846.165	100	15	36.5	35.5
52	578500	3864960	0	50623.171	257.56868	67	6	34	33
53	578500	3864965	0	49802.355	-563.2606	61	2	36	31.5
54	578500	3864970	0	49787.047	-578.58189	59	2	38	30
55	578500	3864975	0	50131.114	-234.52818	53	1	38	30
56	578500	3864980	0	50227.51	-138.14546	46	0.9	38	30
57	578500	3864985	0	50224.972	-140.69676	40	0.2	40.5	29.5
58	578500	3864990	0	50307.851	-57.831041	37	0.02	43	29
59	578500	3864995	0	50346.706	-18.989326	32	0.06	53	29.5
60	578500	3865000	0	50348.989	-16.719611	29	-0.5	63	30
61	578500	3865005	0	50372.368	6.6460983	29	-1	64.5	32
62	578500	3865010	0	50387.893	22.157813	27	-0.09	66	34
63	578500	3865015	0	50240.969	-124.77947	26	-1	59.5	34.5
64	578500	3865020	0	50085.166	-280.59576	28	-1	53	35
65	578500	3865025	0	50046.65	-319.12505	30	0.09	53.5	33
66	578500	3865030	0	50174.264	-191.52433	31	-0.07	54	31
67	578500	3865035	0	50203.526	-162.27562	31	-0.7	55	32
68	578500	3865040	0	50200.067	-165.74791	38	0.3	56	33
69	578500	3865045	0	50206.065	-159.76319	51	1	49.5	31.5
70	578500	3865050	0	50214.998	-150.84348	37	0.2	43	30

Def stn	easting	Northing	Line#	MAG(nT)	IGRF(nT)	Q(mS/m)	I(ppt)	VD(mS/m)	HD(mS/m)
71	578500	3865055	0	50274.053	-91.801763	41	1	47.5	32.5
78	578500	3865090	0	50235.491	-130.45677	46	1	50	38
79	578500	3865095	0	50241.982	-123.97906	44	1	51	40
80	578500	3865100	0	50246.912	-119.06234	50	1	52	42
81	578500	3865105	0	50213.198	-152.78963	45	2	51	43
82	578500	3865110	0	50209.707	-156.29391	57	3	50	44
83	578500	3865115	0	50226.639	-139.3752	56	4	47.5	44.5
84	578500	3865120	0	50208.169	-157.85849	56	4	45	45
85	578500	3865125	0	50058.983	-307.05777	62	5	50	51.5
86	578500	3865130	0	50026.994	-339.06005	39	1	55	58
87	578500	3865135	0	50263.506	-102.56134	55	4	5.5	54
88	578500	3865140	0	50314.246	-51.834628	51	2	-44	50
89	578500	3865145	0	50318.757	-47.336913	49	1	14	43.5
90	578500	3865150	0	50301.868	-64.239203	48	8	72	37
91	578500	3865155	0	50229.765	-136.35549	43	0.3	57.5	37
92	578500	3865160	0	50258.435	-107.69877	43	0.4	43	37
93	578500	3865165	0	50255.487	-110.66006	44	0.2	41	39
94	578500	3865170	0	50257.005	-109.15535	43	0.15	39	41
95	578500	3865175	0	50278.956	-87.217629	46	0.1	39	46
96	578500	3865180	0	50285.843	-80.343913	45	0.001	39	51
97	578500	3865185	0	50401.044	34.843803	50	0.1	9.5	39
98	578500	3865190	0	50285.868	-80.345487	50	-0.9	-20	27
99	578500	3865195	0	50282.41	-83.816771	56	1	14	33
100	578500	3865200	0	50294.181	-72.059055	42	1	48	39
101	578500	3865205	0	50277.847	-88.406344	60	0.1	41.5	50
102	578500	3865210	0	50246.925	-119.34163	49	-7	35	61
103	578500	3865215	0	50293.568	-72.711912	49	0.4	72	106
104	578500	3865220	0	50555.481	189.1878	49	0.4	109	151
105	578500	3865225	0	51468.507	1102.2005	49	0.2	35.5	143.5
106	578500	3865230	0	50521.058	154.73823	50	0.2	-38	136
107	578500	3865235	0	50221.746	-144.58705	49	0.01	-38	108
108	578500	3865240	0	50258.561	-107.78534	47	0.4	-38	80
109	578500	3865245	0	50282.929	-83.430626	46	0.01	23	69
110	578500	3865250	0	50251.9	-114.47291	53	6	84	58
111	578500	3865255	0	50280.288	-86.098193	57	7	85.5	59

Def stn	easting	Northing	Line#	MAG(nT)	IGRF(nT)	Q(mS/m)	I(ppt)	VD(mS/m)	HD(mS/m)
117	578500	3865285	0	50087.945	-278.52091	49	-1	99	58
118	578500	3865290	0	50393.058	26.578812	60	0.1	88	59
119	578500	3865295	0	50307.278	-59.214472	58	1	104	70.5
120	578500	3865300	0	49984.376	-382.12976	20	-6	120	82
121	578500	3865305	0	49532.996	-833.52304	31	-5	77	69
122	578500	3865310	0	48316.051	-2050.4813	89	7	34	56
123	578500	3865315	0	47992.674	-2373.8716	61	1	50	57
124	578500	3865320	0	50219.397	-147.1619	55	0.2	66	58
125	578500	3865325	0	50380.001	13.428817	53	-0.1	61	51
126	578500	3865330	0	51863.615	1497.0295	52	-0.1	56	44
127	578500	3865335	0	50800.378	433.77925	53	-0.1	61.5	49
128	578500	3865340	0	50161.966	-204.64604	55	-0.1	67	54
129	578500	3865345	0	50213.229	-153.39632	56	0.1	48	54
130	578500	3865350	0	50267.768	-98.870603	58	0.2	29	54
131	578500	3865355	0	50308.214	-58.437892	59	0.6	57.5	54.5
132	578500	3865360	0	50324.636	-42.029175	61	1	86	55
133	578500	3865365	0	50310.952	-55.726458	66	2.5	76	51
134	578500	3865370	0	50305.481	-61.210741	74	5	66	47
135	578500	3865375	0	50328.887	-37.81803	65	1	67	43.5
136	578500	3865380	0	50341.834	-24.884312	54	-0.5	68	40
137	578500	3865385	0	50341.635	-25.096595	58	-0.09	65.5	36.5
138	578500	3865390	0	50366.379	-0.3658837	46	-1	63	33
139	578500	3865395	0	50413.658	46.899834	46	-1	28.5	32
140	578500	3865400	0	50478.753	111.98155	49	-1	-6	31
141	578500	3865405	0	50899.357	532.57227	47	-1	31.5	34.5
142	578500	3865410	0	51248.693	881.89498	54	-1	69	38
143	578500	3865415	0	50800.416	433.6047	48	-4	61	39.5
144	578500	3865420	0	51003.777	636.95242	37	-1	53	41
145	578500	3865425	0	50767.534	400.69613	49	-1	58.5	40
146	578500	3865430	0	50357.614	-9.2371557	42	-1	64	39
147	578500	3865435	0	50135.648	-231.21644	37	-1	88.5	42
148	578500	3865440	0	50060.281	-306.59672	34	-1	113	45
149	578500	3865445	0	50006.104	-360.787	31	-1	212	81
150	578500	3865450	0	49911.351	-455.55329	30	-1	311	117

Def stn	easting	Northing	Line#	MAG(nT)	IGRF(nT)	Q(mS/m)	I(ppt)	VD(mS/m)	HD(mS/m)
155	578500	3865475	0	51880.931	1513.9603	37	-1	132.5	249.5
156	578500	3865480	0	51031.093	664.10901	37	-1	-45	205
157	578500	3865485	0	50287.569	-79.428279	39	-0.7	34	161
158	578500	3865490	0	50429.551	62.540439	52	-1	113	117
159	578500	3865495	0	50589.138	222.11416	52	-1	90	100.5
160	578500	3865500	0	51093.52	726.48288	61	4	67	84
161	578500	3865505	0	50557.407	190.35659	49	-3	62	83
162	578500	3865510	0	50160.519	-206.54469	69	2	57	82
163	578500	3865515	0	49928.518	-438.55898	104	7	48.5	79
164	578500	3865520	0	50230.741	-136.34926	82	1	40	76
165	578500	3865525	0	50324.45	-42.653546	107	-20	-5.5	62.5
166	578500	3865530	0	49938.074	-429.04283	117	-20	-51	49
167	578500	3865535	0	48608.359	-1758.7711	192	10	-25.5	24.5
409	578406	3866053	6	49911.903	-458.13707	57	-20	211	30
410	578406	3866058	6	53661.057	3290.9882	22	-16	171	28.5
411	578406	3866063	6	49489.087	-881.01047	58	1	131	27
412	578406	3866068	6	50161.446	-208.68017	46	-1	148	29.5
413	578406	3866073	6	50342.454	-27.700867	43	-1	165	32
414	578406	3866078	6	50205.323	-164.86057	39	-1	229.5	76
415	578406	3866083	6	50261.491	-108.72126	44	-2	294	120
416	578406	3866088	6	50276.546	-93.694963	45	-1	327	186
417	578406	3866093	6	50292.573	-77.696661	42	-2	360	252
418	578406	3866098	6	50280.428	-89.87036	42	-2	198.5	140.5
419	578406	3866103	6	50307.327	-63.000058	40	-2	37	29
420	578406	3866108	6	50333.11	-37.245757	40	-2	40	29
421	578406	3866113	6	50290.961	-79.423455	36	-2	43	29
422	578406	3866118	6	50327.877	-42.536154	34	-2	51	31
423	578406	3866123	6	50085.274	-285.16785	34	-3	59	33
424	578406	3866128	6	50342.539	-27.931551	31	-3	59.5	31
425	578406	3866133	6	50256.828	-113.67125	33	-3	60	29
426	578406	3866138	6	50308.735	-61.792947	31	-3	61.5	30.5
427	578406	3866143	6	50308.446	-62.110646	34	-2	63	32
428	578406	3866148	6	50311.296	-59.289344	32	-2	62.5	31
429	578406	3866153	6	50123.686	-246.92804	32	-3	62	30
430	578406	3866158	6	50268.799	-101.84374	31	-2	63	29

Def stn	easting	Northing	Line#	MAG(nT)	IGRF(nT)	Q(mS/m)	I(ppt)	VD(mS/m)	HD(mS/m)
435	578406	3866183	6	50199.616	-171.17023	29	-2	65	27
436	578406	3866188	6	50258.24	-112.57493	28	-2	63.5	26
437	578406	3866193	6	50372.682	1.8383717	32	-2	62	25
438	578406	3866198	6	50272.543	-98.329326	31	-3	61.5	26
439	578406	3866203	6	50049.565	-321.33602	33	-2	61	27
440	578406	3866208	6	50161.512	-209.41772	32	-2	62	26.5
441	578406	3866213	6	50202.409	-168.54942	29	-2	63	26
442	578406	3866218	6	50210.459	-160.52812	28	-2	54.5	24
443	578406	3866223	6	50189.417	-181.59882	27	-2	46	22
444	578406	3866228	6	50219.371	-151.67352	25	-2	60	20.5
445	578406	3866233	6	50238.775	-132.29821	23	-3	74	19
446	578406	3866238	6	50225.371	-145.73091	22	-3	-0.5	16.5
447	578406	3866243	6	50215.738	-155.39261	22	-3	-75	14
448	578406	3866248	6	50206.148	-165.01131	22	-3	-10	19.5
449	578406	3866253	6	50189.803	-181.38501	22	-3	55	25
450	578406	3866258	6	50269.189	-102.0277	20	-4	58	22
451	578406	3866263	6	50766.844	395.5986	23	-3	61	19
452	578406	3866268	6	49953.644	-417.6301	24	-3	46.5	25.5
453	578406	3866273	6	48623.75	-1747.5528	50	-2	32	32
454	578406	3866278	6	50227.446	-143.88549	18	-3	36	28.5
455	578406	3866283	6	50137.47	-233.89019	33	-2	40	25
456	578406	3866288	6	49776.087	-595.30189	40	-2	41	24.5
457	578406	3866293	6	48944.98	-1426.4376	-15	-5	42	24
458	578406	3866298	6	50353.903	-17.543286	67	-0.2	43.5	24.5
459	578406	3866303	6	55002.852	4631.377	48	-1	45	25
460	578406	3866308	6	49768.773	-602.73068	13	-20	43	25
461	578406	3866313	6	50178.915	-192.61738	43	-0.5	41	25
462	578406	3866318	6	50177.714	-193.84708	34	-1	39.5	26.5
463	578406	3866323	6	50191.996	-179.59377	32	-1	38	28
464	578406	3866328	6	50235.637	-135.98147	34	-1	39	28.5
465	578406	3866333	6	50256.007	-115.64017	29	-2	40	29
466	578406	3866338	6	50279.127	-92.548867	31	-1	40	28
467	578406	3866343	6	50275.54	-96.164565	29	-1	40	27
468	578406	3866348	6	50287.546	-84.187263	29	-1	38	27
469	578406	3866353	6	50283.374	-88.38796	31	-1	36	27

Def stn	easting	Northing	Line#	MAG(nT)	IGRF(nT)	Q(mS/m)	I(ppt)	VD(mS/m)	HD(mS/m)
470	578406	3866358	6	50276.948	-94.842658	33	-1	37	28.5
471	578406	3866363	6	50266.475	-105.34436	23	-1	38	30
472	578406	3866368	6	50364.769	-7.079053	35	-3	37.5	30.5
473	578406	3866373	6	50357.586	-14.290751	37	-2	37	31
474	578406	3866378	6	50357.777	-14.128448	37	-2	38.5	31
475	578406	3866383	6	50370.002	-1.9321455	42	-2	40	31
476	578406	3866388	6	50337.727	-34.235843	40	-2	40	31
477	578406	3866393	6	50336.898	-35.09354	36	-2	40	31
478	578406	3866398	6	50307.193	-64.827238	36	-2	38.5	32
479	578406	3866403	6	50295.379	-76.669935	35	-2	37	33
480	578406	3866408	6	50252.501	-119.57663	38	-2	36	33.5
481	578406	3866413	6	50232.543	-139.56333	34	-2	35	34
482	578406	3866418	6	50286.233	-85.902027	34	-2	35.5	42
483	578406	3866423	6	50278.961	-93.202725	33	-2	36	50
484	578406	3866428	6	50250.498	-121.69442	37	-1	37	39
485	578406	3866433	6	50132.628	-239.59312	42	-5	38	28
486	578406	3866438	6	50140.606	-231.64382	45	-1	37.5	28
650	579100	3866938	11	49460.489	-910.96289	29	-1	160	33
651	579100	3866933	11	50117.459	-253.96162	28	-1	150.5	32
652	579100	3866928	11	50174.457	-196.93235	27	-1	141	31
653	579100	3866923	11	50166.209	-205.14909	26	-1	104	28.5
654	579100	3866918	11	50193.07	-178.25682	26	-1	67	26
655	579100	3866913	11	50212.654	-158.64155	27	-2	103.5	46.5
656	579100	3866908	11	50204.219	-167.04528	29	2	140	67
657	579100	3866903	11	50183.007	-188.22601	33	3	141	60.5
658	579100	3866898	11	50164.612	-206.58975	30	-3	142	54
659	579100	3866893	11	50131.378	-239.79248	29	-1	138.5	58
660	579100	3866888	11	50106.904	-264.23521	12	-20	135	62
661	579100	3866883	11	49944.685	-426.42294	36	0.7	143	69
662	579100	3866878	11	49975.27	-395.80667	21	2	151	76
663	579100	3866873	11	49869.801	-501.24441	45	-0.3	123	76.5
664	579100	3866868	11	49909.831	-461.18314	33	-1	95	77
665	579100	3866863	11	49269.331	-1101.6519	32	-1	56.5	49
666	579100	3866858	11	50198.248	-172.7036	29	-2	18	21
667	579100	3866853	11	50123.771	-247.14933	32	-2	22	19.5

Def stn	easting	Northing	Line#	MAG(nT)	IGRF(nT)	Q(mS/m)	I(ppt)	VD(mS/m)	HD(mS/m)
671	579100	3866833	11	50169.416	-201.37926	31	-2	22.5	16
672	579100	3866828	11	50050.232	-320.53199	30	-2	21	15
673	579100	3866823	11	49894.606	-476.12672	30	-2	21	15.5
674	579100	3866818	11	50302.814	-67.887456	25	-2	21	16
675	579100	3866813	11	50299.492	-71.178188	25	-2	28	15.5
676	579100	3866808	11	50227.689	-142.94992	19	-1	35	15
677	579100	3866803	11	50187.904	-182.70365	18	-2	-7	18
678	579100	3866798	11	50173.241	-197.33538	17	-2	-49	21
679	579100	3866793	11	50163.821	-206.72411	17	-2	70.5	32.5
680	579100	3866788	11	50168.923	-201.59085	16	-2	190	44
681	579100	3866783	11	50172.528	-197.95458	16	-2	126.5	32
682	579100	3866778	11	50201.605	-168.84631	17	-2	63	20
683	579100	3866773	11	50216.192	-154.22804	17	-1	47	19.5
684	579100	3866768	11	50238.933	-131.45577	20	0.5	31	19
685	579100	3866763	11	50258.036	-112.3215	35	4	43.5	29.5
686	579100	3866758	11	50274.241	-96.085236	31	2	56	40
687	579100	3866753	11	50267.23	-103.06497	29	1	27.5	44
688	579100	3866748	11	50246.934	-123.3297	29	0.4	-1	48
689	579100	3866743	11	50187.079	-183.15343	23	-1	19.5	54.5
690	579100	3866738	11	50150.493	-219.70816	17	-2	40	61
691	579100	3866733	11	50147.488	-222.68189	17	-2	41	53
692	579100	3866728	11	50464.773	94.634374	21	-2	42	45
693	579100	3866723	11	50185.434	-184.67336	31	-1	51.5	46.5
694	579100	3866718	11	50197.52	-172.55609	0.7	-9	61	48
695	579100	3866713	11	50176.626	-193.41882	25	-1	-12	54
696	579100	3866708	11	50231.853	-138.16055	19	-2	-85	60
697	579100	3866703	11	50268.204	-101.77828	19	-2	-65.5	66.5
698	579100	3866698	11	50929.96	560.00899	18	-2	-46	73
699	579100	3866693	11	50260.039	-109.88075	18	-2	-21.5	87.5
700	579100	3866688	11	50261.093	-108.79548	20	-2	3	102
701	579100	3866683	11	50209.02	-160.83721	14	-1	8.5	79.5
702	579100	3866678	11	50247.775	-122.05094	41	3	14	57
703	579100	3866673	11	50264.983	-104.81167	-31	-19	35.5	42
704	579100	3866668	11	50278.233	-91.530403	34	1	57	27
705	579100	3866663	11	50253.954	-115.77813	23	-1	61.5	28

Def stn	easting	Northing	Line#	MAG(nT)	IGRF(nT)	Q(mS/m)	I(ppt)	VD(mS/m)	HD(mS/m)
711	579100	3866633	11	50271.558	-97.986522	19	-3	41.5	31
712	579100	3866628	11	50232.468	-137.04525	19	-3	32	30
713	579100	3866623	11	50269.476	-100.00598	19	-2	46.5	30
714	579100	3866618	11	50271.971	-97.479715	16	-2	61	30
715	579100	3866613	11	50265.021	-104.39845	17	-2	60.5	26.5
716	579100	3866608	11	50297.297	-72.091178	16	-2	60	23
717	579100	3866603	11	50295.55	-73.806909	15	-2	65.5	38
718	579100	3866598	11	50237.383	-131.94264	15	-2	71	53
719	579100	3866593	11	50175.104	-194.19037	14	-2	75	52.5
720	579100	3866588	11	50293.221	-76.042102	12	-2	79	52
721	579100	3866583	11	50281.374	-87.857833	13	-2	16.5	50
722	579100	3866578	11	50260.761	-108.43956	15	-2	-46	48
723	579100	3866573	11	50251.948	-117.2213	16	-1	25.5	62
724	579100	3866568	11	50171.693	-197.44503	29	2	97	76
725	579100	3866563	11	50209.499	-159.60776	-37	-24	68.5	74
726	579100	3866558	11	50260.063	-109.01249	34	2	40	72
727	579100	3866553	11	50267.866	-101.17822	24	-1	27.5	52
728	579100	3866548	11	50241.109	-127.90395	22	-1	15	32
729	579100	3866543	11	50206.953	-162.02868	23	-1	19.5	30.5
730	579100	3866538	11	50240.86	-128.09041	27	-2	24	29
731	579100	3866533	11	50168.671	-200.24814	27	-2	18	31.5
732	579100	3866528	11	50202.286	-166.60187	36	0.4	12	34
733	579100	3866523	11	50184.354	-184.50261	21	-1	10	31
734	579100	3866518	11	50318.205	-50.620336	40	0.7	8	28
735	579100	3866513	11	50438.821	70.026933	27	-1	33.5	27
736	579100	3866508	11	50214.026	-154.7368	31	-0.7	59	26
737	579100	3866503	11	49664.463	-704.26853	17	-2	49	26.5
738	579100	3866498	11	50189.521	-179.17926	31	0.4	39	27
739	579100	3866493	11	50183.531	-185.13799	25	-0.7	34.5	28.5
740	579100	3866488	11	50159.282	-209.35572	25	-1	30	30
741	579100	3866483	11	50171.013	-197.59345	27	-1	26.5	32.5
742	579100	3866478	11	50196.51	-172.06518	29	-1	23	35
743	579100	3866473	11	50217.429	-151.11491	30	-1	22.5	34.5
744	579100	3866468	11	50211.158	-157.35464	27	-1	22	34
745	579100	3866463	11	49750.844	-617.63738	26	-1	25	29.5

Def stn	easting	Northing	Line#	MAG(nT)	IGRF(nT)	Q(mS/m)	I(ppt)	VD(mS/m)	HD(mS/m)
746	579100	3866458	11	48984.323	-1384.1271	22	-1	28	25
747	579100	3866453	11	48355.831	-2012.5878	22	-1	27.5	24.5
748	579100	3866448	11	49238.395	-1129.9926	21	-1	27	24
749	579100	3866443	11	50179.834	-188.5223	20	-1	26.5	27
750	579100	3866438	11	50293.981	-74.344029	19	-1	26	30
751	579100	3866433	11	50275.054	-93.23976	20	-1	24.5	24
752	579100	3866428	11	50273.791	-94.47149	22	-1	23	18
753	579100	3866423	11	50259.48	-108.75122	28	-1	-122.5	67.5
754	579100	3866418	11	50306.149	-62.050951	26	-2	-268	117
755	579100	3866413	11	50293.321	-74.847682	57	2	-131.5	73
756	579100	3866408	11	50253.847	-114.29041	80	11	5	29
757	579100	3866403	11	50234	-134.10614	51	7	71	47
758	579100	3866398	11	50196.385	-171.68987	50	4	137	65
759	579100	3866393	11	50129.676	-238.3676	50	5	179	97.5
760	579100	3866388	11	50089.73	-278.28233	41	3	221	130
761	579100	3866383	11	50137.603	-230.37807	41	3	200	98
762	579100	3866378	11	50198.008	-169.9418	47	4	179	66
763	579100	3866373	11	50244.359	-123.55953	47	3	154	68.5
764	579100	3866368	11	50267.45	-100.43726	44	3	129	71
765	579100	3866363	11	50247.638	-120.21799	37	3	130	67.5
766	579100	3866358	11	50394.542	26.717282	34	3	131	64
767	579100	3866353	11	53091.158	2723.3646	31	2	136	68
768	579100	3866348	11	49967.94	-399.82218	32	3	141	72
769	579100	3866343	11	48857.497	-1510.2339	34	2	151.5	85
770	579100	3866338	11	45297.049	-5070.6506	38	3	162	98
771	579100	3866333	11	46610.786	-3756.8824	36	2	147	163
772	579100	3866328	11	48133.722	-2233.9151	24	-1	132	228
773	579100	3866323	11	49678.525	-689.08083	25	-1	81	152
774	579100	3866318	11	50220.337	-147.23756	111	0.4	30	76
775	579100	3866313	11	50322.524	-45.019291	62	3	157.5	67.5
776	579100	3866308	11	50269.187	-98.325021	54	-2	285	59

Def stn	easting	Northing	Line#	MAG(nT)	IGRF(nT)	Q(mS/m)	I(ppt)	VD(mS/m)	HD(mS/m)
786	579100	3866258	11	50486.385	119.18568	53	-1	174	40
787	579100	3866253	11	50313.575	-53.593054	54	-1	130	39
788	579100	3866248	11	50204.108	-163.02878	43	-2	86	38
789	579100	3866243	11	50244.646	-122.45951	44	-1	76.5	38
790	579100	3866238	11	50227.126	-139.94824	39	-1	67	38
791	579100	3866233	11	50275.76	-91.282974	37	-1	68	36.5
792	579100	3866228	11	50273.806	-93.205704	35	-2	69	35
793	579100	3866223	11	50314.339	-52.641434	35	-2	78.5	32
794	579100	3866218	11	50294.005	-72.944164	36	-1	88	29
795	579100	3866213	11	50246.845	-120.07289	41	0.7	92	30
796	579100	3866208	11	50261.518	-105.36862	46	-2	96	31
797	579100	3866203	11	50259.685	-107.17035	45	1	115.5	30
798	579100	3866198	11	50260.648	-106.17608	45	1	135	29
799	579100	3866193	11	50270.48	-96.312814	38	-1	114.5	56
800	579100	3866188	11	50317.979	-48.782544	33	-1	94	83
801	579100	3866183	11	50243.249	-123.48127	34	-1	64	110
802	579100	3866178	11	50205.633	-161.066	37	-1	34	137
803	579100	3866173	11	50206.266	-160.40173	40	-1	19.5	121
804	579100	3866168	11	50274.526	-92.110464	33	-2	5	105
805	579100	3866163	11	50292.253	-74.352194	29	-1	19	68
806	579100	3866158	11	50380.277	13.703076	26	-1	33	31
807	579100	3866153	11	50312.315	-54.227654	25	-2	52	175.5
808	579100	3866148	11	50382.187	15.675617	26	-2	71	320
809	579100	3866143	11	50272.75	-93.730113	24	-2	67	173.5
810	579100	3866138	11	50283.64	-82.808843	23	-2	63	27
811	579100	3866133	11	50269.123	-97.294573	21	-2	45.5	25
812	579100	3866128	11	50246.763	-119.6233	21	-2	28	23
813	579100	3866123	11	50211.962	-154.39303	21	-2	27	23
814	579100	3866118	11	50176.891	-189.43276	21	-2	26	23
815	579100	3866113	11	50194.297	-171.99549	21	-2	26	23
816	579100	3866108	11	49341.198	-1025.0632	22	-2	26	23
817	579100	3866103	11	50301.24	-64.989951	22	-2	25.5	22.5
818	579100	3866098	11	50545.628	179.42932	24	-2	25	22
819	579100	3866093	11	50278.641	-87.526411	24	-2	25.5	23
820	579100	3866088	11	50086.809	-279.32714	26	-2	26	24

Def stn	easting	Northing	Line#	MAG(nT)	IGRF(nT)	Q(mS/m)	I(ppt)	VD(mS/m)	HD(mS/m)
824	579100	3866068	11	50157.534	-208.47706	35	-2	29	26
825	579100	3866063	11	50079.299	-286.68079	34	-2	30.5	26
826	579100	3866058	11	49741.148	-624.80052	33	-2	32	26
827	579100	3866053	11	47504.194	-2861.7232	38	-2	26.5	27.5
828	579100	3866048	11	50187.374	-178.51198	30	-2	21	29
829	579100	3866043	11	50319.923	-45.931707	31	-2	23.5	29.5
830	579100	3866038	11	50754.085	388.26156	31	-2	26	30
831	579100	3866033	11	50348.67	-17.122166	30	-2	25	31
832	579102.5	3866031	11	50363.741	-2.0198951	27	-2	24	32
833	579105	3866028	11	50313.376	-52.353625	25	-2	23	31
834	579107.5	3866026	11	50303.252	-62.446354	27	-2	22	30
835	579110	3866023	11	50326.009	-39.658083	29	-1	20.5	29.5
836	579112.5	3866021	11	50313.444	-52.191813	27	-1	19	29
837	579115	3866018	11	50290.482	-75.122542	28	-2	19.5	28
838	579117.5	3866016	11	50285.147	-80.426272	30	-2	20	27
839	579120	3866013	11	50208.421	-157.121	30	-2	21.5	28
840	579122.5	3866011	11	50989.055	623.54427	30	-2	23	29
841	579125.5	3866006	11	50054.614	-310.86546	31	-2	23.5	31
842	579128.5	3866001	11	50798.371	432.92281	32	-2	24	33
843	579131.5	3865996	11	49869.871	-495.54592	34	-2	24.5	33
844	579134.5	3865991	11	50183.063	-182.32265	34	-2	25	33
845	579137.5	3865986	11	50129.319	-236.03538	34	-2	25	33.5
846	579140	3865981	11	49908.66	-456.66311	39	-2	25	34
847	579140	3865976	11	49957.239	-408.05284	37	-2	24.5	35
848	579140	3865971	11	50387.87	22.609435	29	-2	24	36
849	579140	3865966	11	50350.875	-14.354294	29	-2	21	34
850	579140	3865961	11	50354.802	-10.396023	24	-2	18	32
851	579140	3865956	11	50415.848	50.681247	22	-2	21	30
852	579140	3865951	11	50452.044	86.908518	20	-2	24	28
853	579140	3865959	11	50971.914	606.80979	23	-2	24.5	26
854	579139	3865949	11	50054.754	-310.31894	24	-2	25	24
855	579138	3865947	11	49869.572	-495.46967	25	-2	24.5	23.5
856	579137	3865945	11	49994.441	-370.5694	29	-2	24	23
857	579136	3865943	11	50287.899	-77.080128	32	-1	25	23.5

Def stn	easting	Northing	Line#	MAG(nT)	IGRF(nT)	Q(mS/m)	I(ppt)	VD(mS/m)	HD(mS/m)
858	579135	3865941	11	50306.222	-58.725857	33	-1	26	24
859	579134	3865939	11	50304.968	-59.948586	34	-1	22	26
860	579133	3865937	11	50299.983	-64.902315	31	-1	18	28
861	579132	3865935	11	50333.678	-31.176044	28	-1	21.5	29.5
862	579131	3865933	11	50255.451	-109.37177	32	-1	25	31
863	579130	3865931	11	49773.389	-591.4025	32	-1	13	31
864	579129	3865929	11	47395.764	-2968.9962	35	-2	1	31
865	579128	3865927	11	50072.549	-292.17996	32	-1	16	31.5
866	579127	3865925	11	50250.002	-114.69569	27	-1	31	32
867	579126	3865923	11	50247.076	-117.59042	28	-1	30.5	30
868	579125	3865922	11	50234.591	-130.04415	26	-2	30	28
869	579124	3865920	11	50250.9	-113.70388	27	-1	31.5	28
870	579123	3865919	11	50264.13	-100.4426	24	-2	33	28
871	579122	3865918	11	50255.6	-108.94133	29	-1	33	36
872	579122	3865913	11	50200.538	-163.97206	29	-1	33	44
873	579122	3865908	11	50208.285	-156.19379	31	-1	20.5	55.5
874	579122	3865903	11	50190.934	-173.51352	34	-1	8	67
875	579122	3865898	11	50092.094	-272.32225	39	-0.9	29.5	61
876	579122	3865893	11	49867.726	-496.65898	47	-1	51	55
877	579122	3865888	11	50179.748	-184.60571	51	-1	35.5	48.5
878	579122	3865883	11	50273.706	-90.616436	26	-5	20	42
879	579122	3865878	11	50273.654	-90.637165	26	-5	28.5	38
880	579122	3865873	11	50245.642	-118.61789	31	-1	37	34
881	579122	3865868	11	50243.902	-119.84358	41	-1	33	34
882	579122	3865863	11	50187.995	-175.70646	37	-1	29	34
883	579122	3865858	11	50081.13	-282.52734	41	-1	18.5	33.5
884	579122	3865853	11	50163.316	-200.29723	45	-1	8	33
885	579117	3865853	11	50384.785	21.215893	56	-1	21.5	33
886	579112	3865853	11	50422.277	58.75201	36	-2	35	33
887	579107	3865853	11	50254.23	-109.25087	34	-1	28	31.5
888	579102	3865853	11	50210.96	-152.47675	29	-2	21	30

Def stn	easting	Northing	Line#	MAG(nT)	IGRF(nT)	Q(mS/m)	I(ppt)	VD(mS/m)	HD(mS/m)
889	579097	3865853	11	50149.663	-213.72964	32	-1	36	33.5
890	579092	3865853	11	50221.692	-141.65652	32	-1	51	37
891	579087	3865853	11	50235.272	-127.82685	32	-1	81.5	42.5
892	579082	3865853	11	50214.915	-148.13203	31	-1	112	48
893	579077	3865853	11	50244.564	-118.48259	41	-1	120	55.5
894	579072	3865853	11	50228.644	-134.40215	37	-1	128	63
895	579067	3865853	11	50156.7	-206.32002	41	-1	133.5	59.5
896	579062	3865853	11	50109.009	-253.95919	45	-1	139	56
897	579057	3865853	11	49953.983	-408.98475	56	-1	103	54
898	579052	3865853	11	49269.532	-1093.4353	36	-2	67	52
899	579047	3865853	11	48226.037	-2136.9299	34	-1	43.5	49
900	579047	3865858	11	49775.292	-587.67444	29	-2	20	46
901	579047	3865863	11	49555.81	-807.156	32	-1	37	45.5
902	579047	3865768	11	49980.391	-382.57456	32	-1	54	45

Appendix 2

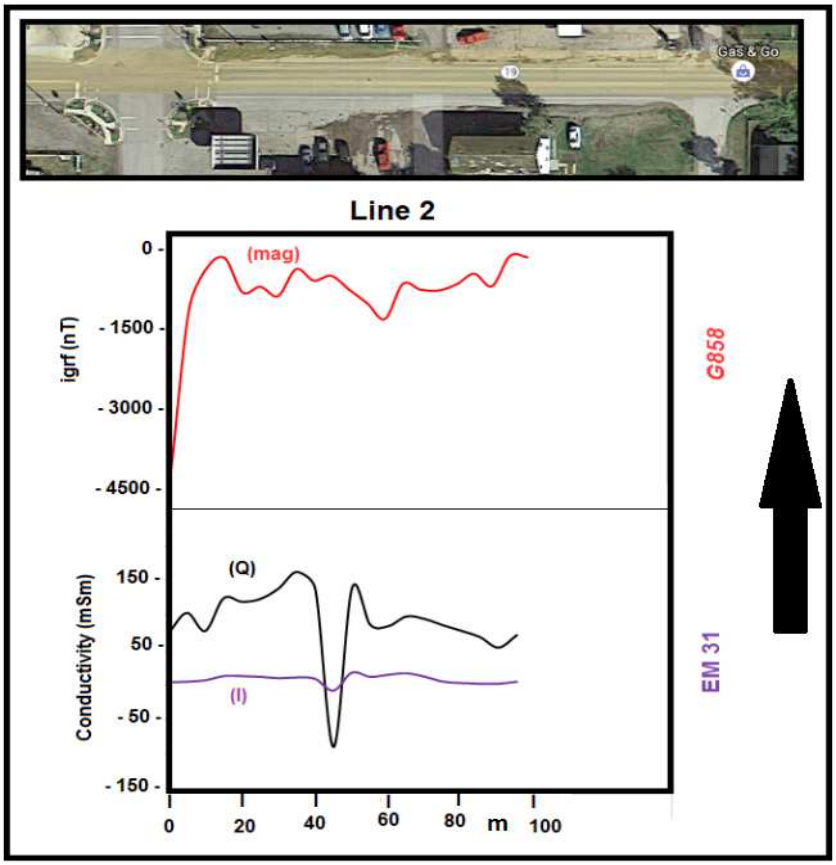

Appendix 2: Electromagnetic and magnetic surveys with EM 31, G858 Magnetometer along the Line 2. Adapted from google map.

Appendix 3

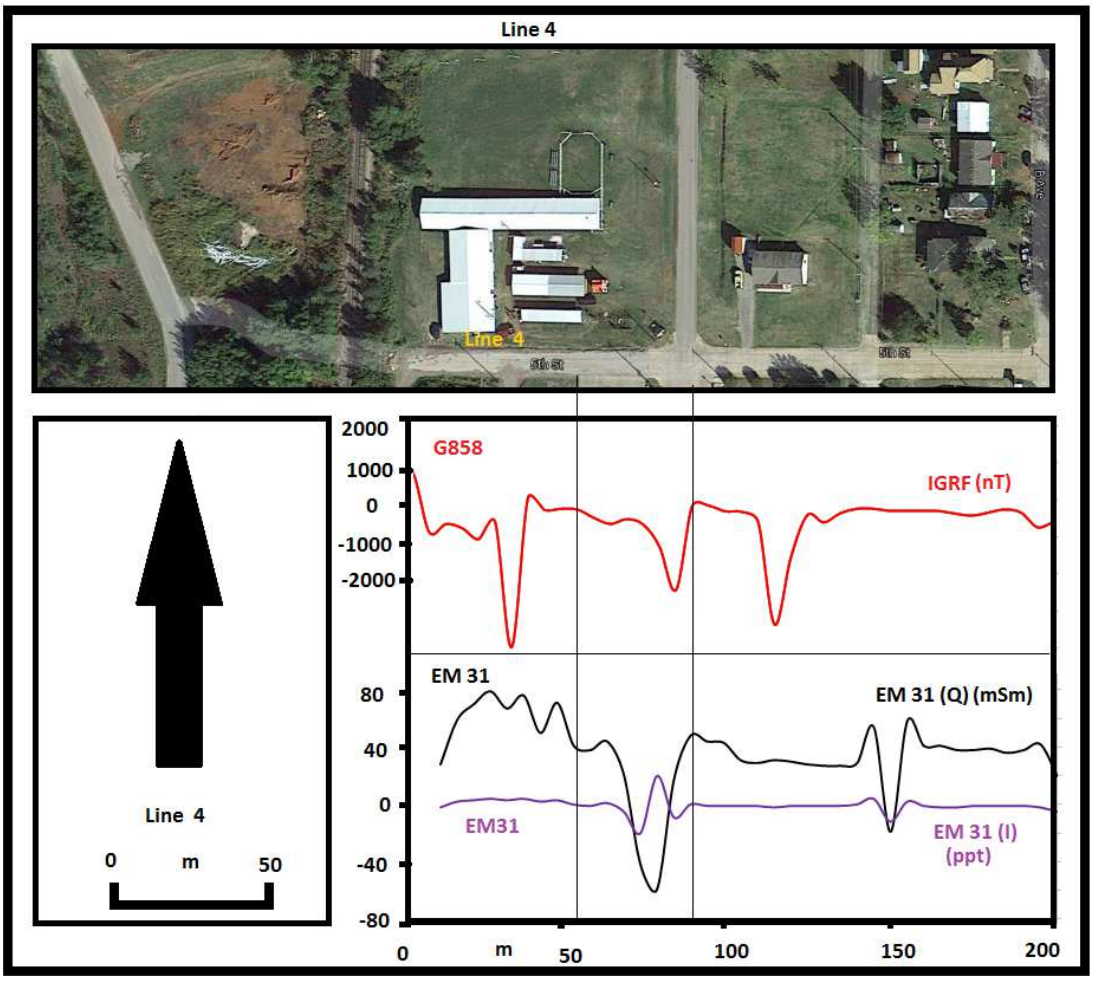

Appendix 3: Electromagnetic and magnetic surveys with EM 31 and G858 cesium magnetometer along the 5th Street (Line 4). Adapted from google map.

Appendix 4

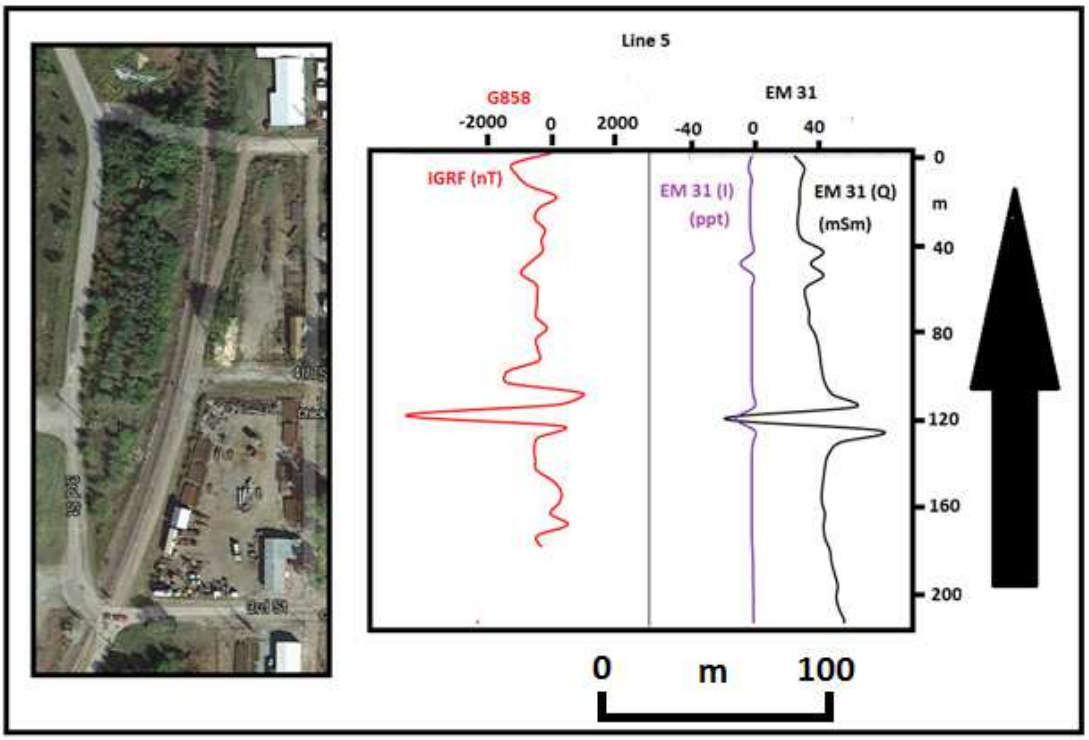

Appendix 4: Electromagnetic and magnetic survey with EM 31 and G858 magnetometer along the Line 5. Picture adapted from the google map.

Appendix 5

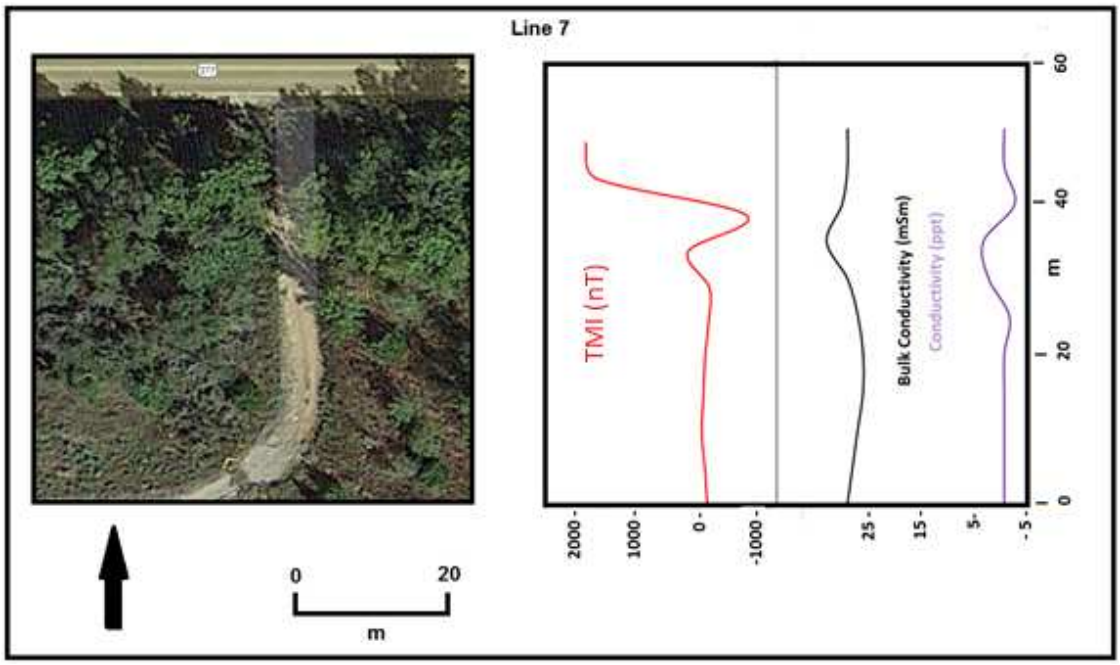

Appendix 5: Electromagnetic and magnetic survey with EM 31 and G858 magnetometer along the Line 7. Picture adapted from the google map.

Appendix 6

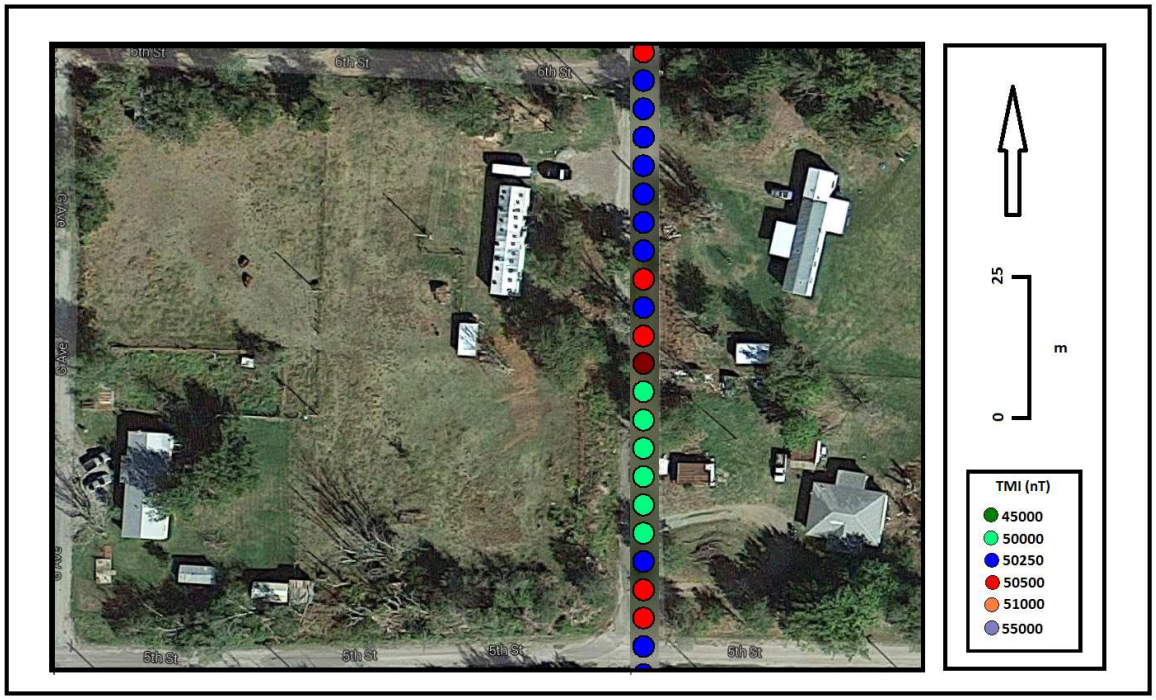

Appendix 6: Magnetic survey with G858 magnetometer along the Line 11. Picture adapted from the google map.

APPENDICES

Annex- 1

Def stn	Easting	Northing	Line#	MAG(nT)	IGRF(nT)	Q(mS/m)	I(mS/m)	VD(mS/m)	HD(mS/m)
0	578500	3864700	0	49851.585	-513.32636	64	20	67	41
1	578500	3864705	0	50131.497	-233.42764	60	20	55.5	41
2	578500	3864710	0	50112.862	-252.07593	40	4	44	41
3	578500	3864715	0	50125.096	-239.85522	46	1	42.5	42
4	578500	3864720	0	50196.454	-168.51051	43	-1	41	43
5	578500	3864725	0	50220.942	-144.0358	45	0.2	38	43
6	578500	3864730	0	50250.616	-114.37509	43	0.7	35	43
7	578500	3864735	0	50259.621	-105.38338	43	-0.1	38.5	44
8	578500	3864740	0	50261.703	-103.31466	42	-1	42	45
9	578500	3864745	0	50254.814	-110.21695	42	-1	38.5	45
10	578500	3864750	0	50245.923	-119.12124	44	-1	35	45
11	578500	3864755	0	50207.87	-157.18753	47	-1	56	45
12	578500	3864760	0	50166.56	-198.51081	51	-1	77	45
13	578500	3864765	0	49966.663	-398.42111	61	-0.3	-1	43
14	578500	3864770	0	45800.135	-4564.9624	72	0.1	-79	41
15	578500	3864775	0	43732.004	-6633.1067	80	1	-16.5	43.5
16	578500	3864780	0	48290.132	-2074.992	70	0.9	46	46
17	578500	3864785	0	50562.857	197.71974	60	0.1	50	45.5
18	578500	3864790	0	50202.708	-162.44255	47	-1	54	45
19	578500	3864795	0	50163.183	-201.98083	41	-1	65.5	45.5
20	578500	3864800	0	50159.333	-205.84412	37	-1	77	46
21	578500	3864805	0	50200.268	-164.92241	40	-0.9	21	44
22	578500	3864810	0	50228.356	-136.8477	47	0.1	-35	42
23	578500	3864815	0	50199.752	-165.46498	18	-3	6.5	48
24	578500	3864820	0	50182.673	-182.55727	52	0.4	48	54
25	578500	3864825	0	50122.528	-242.71556	46	-0.5	46	54.5

VITA

Vincent Tambwe Somwe

Candidate for the Degree of

Master of Science

Thesis: INVESTIGATING THE USE OF GEOPHYSICAL TECHNIQUES FOR DETECTING HYDROCARBON SEEPS

Major Field: Geology

Biographical:

Education:

Completed the requirements for the Master of Science in Geology at Oklahoma State University, Stillwater, Oklahoma in December, 2015.

Completed the requirements for the Bachelor of Mineral Science at University of Zambia, Lusaka, Zambia in 1998.

Experience:
-Teaching Assistant
-Research Assistant
-Wellsite Geologist
-Regional Mapping Geologist

Professional Memberships:
-GSA: Geological Society of America
-SEG: Society of Exploration Geophysicists

[i] Year the website has been accessed